

# A Reconfigurable Electrode Array for Use in Rotational Electrical Impedance Myography

by

Michael Scharfstein

S.B., Electrical Engineering and Computer Science  
Massachusetts Institute of Technology, 2006

Submitted to the Department of Electrical Engineering and Computer Science

in Partial Fulfillment of the Requirements for the Degree of  
Master of Engineering in Electrical Engineering and Computer Science

at the

MASSACHUSETTS INSTITUTE OF TECHNOLOGY

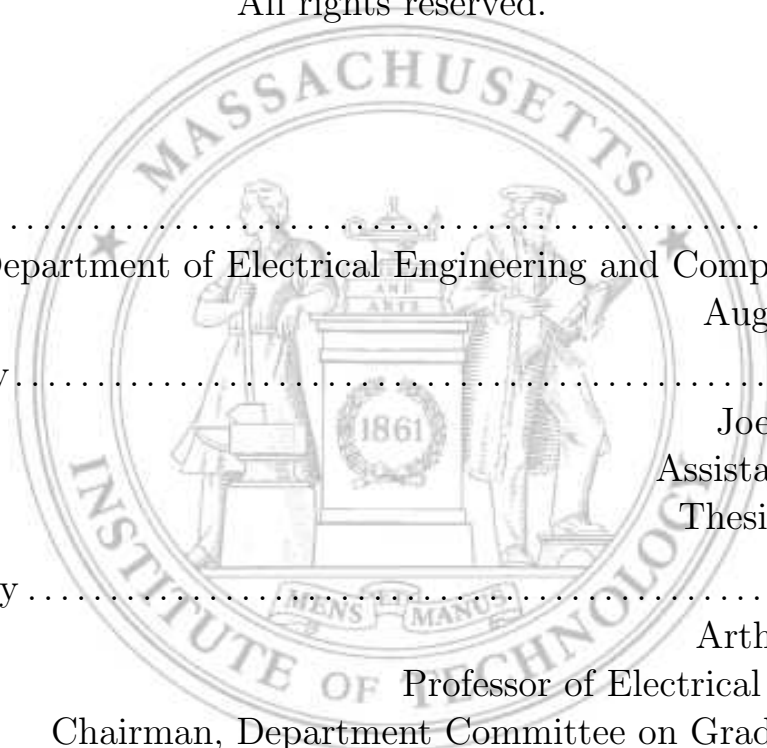
September 2007

© Massachusetts Institute of Technology 2007  
All rights reserved.

Author .....  
Department of Electrical Engineering and Computer Science  
August 21, 2007

Certified by .....  
Joel L. Dawson  
Assistant Professor  
Thesis Supervisor

Accepted by .....  
Arthur C. Smith  
Professor of Electrical Engineering  
Chairman, Department Committee on Graduate Theses





# A Reconfigurable Electrode Array for Use in Rotational Electrical Impedance Myography

by

Michael Scharfstein

Submitted to the  
Department of Electrical Engineering and Computer Science

August 21, 2007

In Partial Fulfillment of the Requirements for the Degree of  
Master of Engineering in Electrical Engineering and Computer Science

## **Abstract**

This thesis describes the design of a novel handheld electrode probe and measurement system for use in rotational electrical impedance myography (EIM), which is a method for diagnosing neuromuscular disease. The probe can be controlled from a PC via USB and uses an array of small electrode cells that can be connected together into larger electrodes with the help of crosspoint switches. A measurement system capable of fast multi-frequency impedance measurement has also been developed. The two systems have performed well, with measurements being very close to those achieved by more traditional electrical impedance myography methods.

Thesis Supervisor: Joel L. Dawson  
Title: Assistant Professor



## Acknowledgments

First and foremost, I would like to thank my research advisor, Prof. Joel L. Dawson. I first met him as one of the instructors in my feedback systems course, which he made a pleasure to take due to his enthusiasm and aptitude for teaching. He has continued to be a wonderful advisor and mentor, and I wish to thank him for giving me the opportunity to work on this project. His help, patience, and encouragement have made this a wonderful experience.

I would also like to thank Dr. Seward B. Rutkove, without whom this project would never have existed, for his excitement and expertise for electrical impedance myography. He, along with Drs. Andrew Tarulli, Ron Aaron, and Carl Shiffman, has been key components in both the past and present stages of this project.

I wish the other members of the EIM group, Muyiwa Oginnika and Roshni Cooper, good luck and success as they continue working on this project. I must acknowledge their huge contributions to this project, especially Muyiwa who has worked extensively on the impedance measurement system.

Finally, I would like to thank my family and friends for their continual love and support.



# Contents

<b>1</b>	<b>Introduction</b>	<b>13</b>
1.1	Neuromuscular Disorders . . . . .	14
1.2	Neuromuscular Diagnostic Methods . . . . .	15
1.3	Variants of Electrical Impedance Myography . . . . .	17
1.4	Concept of Electrical Impedance Myography . . . . .	19
1.5	Goals and Organization of this Work . . . . .	22
<b>2</b>	<b>Impedance Measurement</b>	<b>25</b>
2.1	Equipment, Circuits, and Methods . . . . .	27
2.2	Input Waveform . . . . .	30
2.2.1	Waveform Type . . . . .	31
2.2.2	Frequency Spacing . . . . .	32
2.3	Performance . . . . .	34
2.3.1	Sources of Error . . . . .	35
<b>3</b>	<b>Electrode Probe Design</b>	<b>39</b>
3.1	Testing Methods . . . . .	40
3.2	Electrode Probe Prototypes . . . . .	41
3.2.1	Electrode Arrays . . . . .	42
3.2.2	Prototype Design . . . . .	45
3.2.3	Prototype Results . . . . .	45
3.3	Final Design . . . . .	48
3.3.1	Electrode Array . . . . .	49

3.3.2	Switching . . . . .	51
3.3.3	Controller . . . . .	55
3.3.4	Power Supplies . . . . .	56
3.3.5	Software . . . . .	57
3.3.6	Performance . . . . .	61
<b>4</b>	<b>Patient Safety</b>	<b>65</b>
4.1	Cardiac Concerns . . . . .	65
4.2	Isolation . . . . .	66
4.3	Current Density . . . . .	66
<b>5</b>	<b>Conclusion</b>	<b>67</b>
5.1	Future Work . . . . .	68

# List of Figures

1-1	A Comparison of linear and rotational electrical impedance myography measurements being performed on a patient. . . . .	19
1-2	A network model of muscle. . . . .	19
1-3	Simplified muscle network. . . . .	20
1-4	Skeletal muscle magnified 200x. . . . .	21
2-1	Electrical impedance myography instrument currently being used at Beth Israel Deaconess Hospital . . . . .	26
2-2	Equipotentials and current flow for a tetrapolar impedance measurement	27
2-3	System diagram of the prototype measurement setup . . . . .	28
2-4	Schematic of the electrode probe driver. . . . .	28
2-5	Comparison of measurements of a $100\Omega$ resistor using different amounts of averaging. . . . .	30
2-6	A Comparison of composite input waveforms . . . . .	33
2-7	Comparison of the ideal and measured impedance of a five element muscle model with the parameters in Table 2.1 . . . . .	36
2-8	The effect of impedance magnitude on the perception of parasitics . .	36
3-1	An early electrode array design: superposition of electrode strips. . .	42
3-2	Concept of electrode array with virtual electrodes “drawn” on. . . . .	43
3-3	A passive averager circuit. . . . .	44
3-4	Rectangular electrode probe prototypes. . . . .	45
3-5	A comparison of bode plots of balsa wood as measured using 400mil rectangular prototype and electrode strips. . . . .	46

3-6	The effect of gel coverage on observed anisotropy in balsa wood. . . .	47
3-7	Placement of central electrode and resultant current paths in layered tissue. . . . .	48
3-8	Illustrations of the complete electrode probe. . . . .	49
3-9	Illustrations of the controller module . . . . .	51
3-10	A photograph of the switching module circuit board. . . . .	53
3-11	A photograph of the analog terminals of two switching modules stacked together. . . . .	54
3-12	Illustrations of the controller module. . . . .	55
3-13	A photograph of the analog power supply module. . . . .	57
3-14	Examples of the three layers of abstraction in XML configurations. . .	60
3-15	Screen shots of the electrode probe application suite. . . . .	61
3-16	electrode probe performance compared to electrode strip measurements.	62
3-17	Rotational measurements of balsa wood with electrode probe. . . . .	63

# List of Tables

2.1	Parameters for the 5-element muscle model circuit used in testing. . .	34
-----	--	----



# Chapter 1

## Introduction

Electrical impedance myography (EIM) is a non-invasive technique for neuromuscular assessment originally developed by Dr. Seward Rutkove [18] of Beth Israel Deaconess Medical Center and Drs. Ronald Aaron and Carl Shiffman of Northeastern University. There currently exists a system that performs electrical impedance myography measurements at Beth Israel Deaconess Medical Center. Although it is sufficient to prove the value of electrical impedance myography, it is too slow and cumbersome to realize the full potential of electrical impedance myography as a diagnostic medical tool. This thesis describes the design and testing of a reconfigurable electrode probe, which is capable of taking measurements at many orientations relative to the direction of the fibers of the muscle of interest. Many improvements have been made in this project over the system currently in use. The electrode probe has been reduced to a handheld device for convenience and portability. The speed of measurement has increased dramatically by simultaneously measuring all frequencies of interest. Finally, the electrode probe can be reconfigured to take many different measurements by a computer and without the need to physically change anything.

Electrical impedance myography enables the detection of degenerative neuromuscular diseases such as amyotrophic lateral sclerosis (Lou Gehrigs disease) and inclusion body myositis. In this technique, a low-intensity alternating current is applied to a muscle and the consequent surface voltage patterns are evaluated. From these patterns one can calculate the bulk tissue impedance of the underlying muscle and make

inference about its structure.

## 1.1 Neuromuscular Disorders

Neuromuscular disorders form a group of syndromes that vary widely in both symptoms and pathologies. However, they all lead to some degradation of muscle function and sensory loss, and are often debilitating. Neuromuscular disorders can be divided into three groups:

**Neurogenic Disorders** The nerves that conduct signals between the muscles and the spinal cord and brain are affected in these disorders. They can be diseases that affect the whole body, such as amyotrophic lateral sclerosis, or more localized conditions such as carpal tunnel syndrome. Although these disorders originate in the neurons connected to muscles, the muscles themselves are often affected because they stop being used normally.

**Myopathies** These types of disorders originate in the muscles themselves to prevent their normal function. Often they are characterized by physical changes in the muscle structure. The muscle can get inflamed, or be replaced by scar tissue or fat. It can also become hypertrophic, growing larger than normal to the point of becoming dangerous. Myopathies are very well suited for electrical impedance myography as there is often a physical change in muscle structure that can be detected.

**Disuse Atrophies** The body does not like to keep tissue around that is not being used, as it requires many resources. Accordingly, the body quickly metabolizes excessive muscle that is not exercised sufficiently. This can occur if a patient is bed-bound, has a cast put on a limb, or has a central nervous system problem. Sustaining muscle tone and mass is also a major problem for astronauts on prolonged space-flight [11]. Although strength tests can be done to determine the level of atrophy, the degree of human effort can be hard to quantify and makes the test more subjective than electrical impedance myography.

There is also a group of disorders that affects the junction between neurons and muscles and prevents them from functioning properly. This group is rare and usually not diagnosable using electrical techniques.

## 1.2 Neuromuscular Diagnostic Methods

There are a variety of methods that are currently used to diagnose neuromuscular diseases. Each of them has their own advantages and disadvantages compared to electrical impedance myography, and a combination of methods is often used to make the final diagnosis. Below I will discuss the more popular methods and their limitations.

**Electromyography** Also known as an EMG, this is one of the most common tests performed on a patient who is having neuromuscular problems. There are two forms of electromyography. The first is an invasive form in which needles are inserted through the skin, directly into the muscle. The second, non-invasive form, utilizes surface electrodes placed onto the skin. Both forms of electromyography attempt to detect the small potential changes in muscle caused by neural activity and muscle activation. While these techniques have been used for some time, they have some disadvantages when compared to electrical impedance myography. One clear disadvantage of needle electromyography is that the technique requires the insertion of needles into the patient, which can be very painful and may cause infection. Although surface electromyography is non-invasive like electrical impedance myography, it is subject to disturbances from sources of electrical activity inside and outside of the body such as from the heart or from power lines.

**Magnetic Resonance Imaging** Magnetic resonance imaging (MRI) is sometimes used to look for structural defects in muscle and for nerve displacement or damage in the spine. MRI is also used to help with the choice of a proper site for a biopsy [16]. However, due to MRI's expense, and the large amount of data it produces, it has only gained limited use for this particular purpose. In

addition, it would be difficult to perform tests on dynamic muscle performance where the patient uses the muscle to perform a task. This would be difficult because MRI machines are very confining, and they operate on relatively long timescales.

**Ultrasound** Ultrasound been used to find muscle inflammation [17] and nerve compression [9]. Ultrasound also has the drawback of being a very qualitative technique in which differences in individual physicians' techniques can cause major changes in the resulting images.

**Biopsy** A muscle biopsy is usually used to find an exact diagnosis of a neuromuscular disease. A biopsy is a surgical technique where a small part of the muscle of interest is removed to be studied further in a lab. Although a biopsy is regarded as the gold standard, it can be an inconclusive test since myopathies do not always occur homogeneously in a muscle. The result is that many biopsies may need to be taken to obtain a diagnosis.

**Other Methods** Other tests exist to diagnose neuromuscular disease, including blood tests, new imaging techniques, and genetic screenings. Many of these techniques have proven to assist with the diagnosis of hereditary neuromuscular problems [13].

Electrical impedance myography differs from the classical techniques for neuromuscular assessment, mentioned above, in many ways. Electrical impedance myography is an active measurement, while most other techniques try to measure naturally occurring potential changes passively. This is done by passing a low intensity alternating current through the tissue and then measuring the voltage drop across it instead of trying to passively measure the minute voltage changes produced by the body itself. It is of interest to us because it is a more direct measure of muscle composition than electromyography, which essentially measures muscle activity. Since the technique attempts to measure the composition of muscle, it would be most suited for assessing myopathies or disuse atrophies. These measurements can be taken painlessly and

non-invasively using electrodes that are placed on top of the skin. They can also be taken from different parts of the body at the bed side. The previously mentioned attributes make electrical impedance myography a valuable tool that will be able to provide valuable quantitative data, quickly, with little patient discomfort.

### 1.3 Variants of Electrical Impedance Myography

Electrical impedance myography can be performed in a number of different ways to evaluate tissues. All of these techniques pass a current through parts of a patient's body, and measure the voltage that is developed across another part. Perhaps the first distinction that needs to be made is between muscle-specific and whole-body electrical impedance myography. Whole-body electrical impedance myography, also known as bioelectrical impedance, can be used to determine the rough composition of the body and has been around since the 1930s. Typically, impedance is measured at one frequency (usually 50 kHz) with the voltage leads far apart and closer to the current leads than to each other. This method is usually used to determine body composition, such as the percentage of the body that is made up of water, or fat [6]. This technique is of little use for diagnosing neuromuscular disease as the results represent a large portion of the body, much of which is not muscle much less the specific muscle of interest.

Muscle-specific electrical impedance myography focuses on determining the composition of one muscle, or a small group of muscles. The goal here is to isolate the impedance of the muscle as much as possible from the impedance of other body tissues, and these techniques work best on muscles which are close to the surface of the body and covered by only small layers of skin and fat tissue. The voltage electrodes are placed directly above the muscle of interest, but the placement of the current electrodes is less critical. The different variations of muscle-specific electrical impedance myography are explained below.

**Linear EIM** Linear electrical impedance myography involves placing multiple pairs of voltage electrodes in a line directly above the muscle or muscle group of

interest. The current electrodes are placed so that current must flow in parallel to this line. The voltages at each point along the muscle are compared during analysis. Both single frequency, 50 kHz, and multi-frequency measurements can be taken. An example of patient preparation can be seen in Figure 1-1(a).

**Rotational EIM** This method, the main focus of this thesis, attempts to characterize the anisotropy of muscle by measuring impedance at multiple angles relative to the direction of muscle fibers. In this case, both the current and voltage electrodes need to be rotated as they must be kept in line with each other at all angles to control the direction of current flow. Multi-frequency measurements are usually taken for the rotational method and then the average phase across all frequencies is compared at each different angle [1,19]. An example of patient preparation can be seen in Figure 1-1(b).

**Dynamic EIM** Dynamic measurements are meant to characterize muscle while it is being active. This may mean using either rotational or linear electrical impedance myography and taking measurements repeatedly as the patient contracts and relaxes his muscle. The measurements can then be compared, perhaps with the addition of data from a force transducer. This method requires the ability to perform measurements quickly as it may be difficult for a patient, especially a sick one, to maintain constant muscle contraction for more than a few seconds.

Dynamic EIM is a relatively new idea, with preliminary work being done by Shiffman et al. in 2003 [20]. However, that work was only done with a linear, single frequency method at 50 kHz. Shiffman et al. specifically mention multi-frequency measurements as one of the future goals for dynamic EIM, stating that current systems do not have enough temporal resolution to make multi-frequency measurements useful. Our system has the potential of providing the features needed to make multi-frequency dynamic EIM a reality, and augment it with rotational measurements.

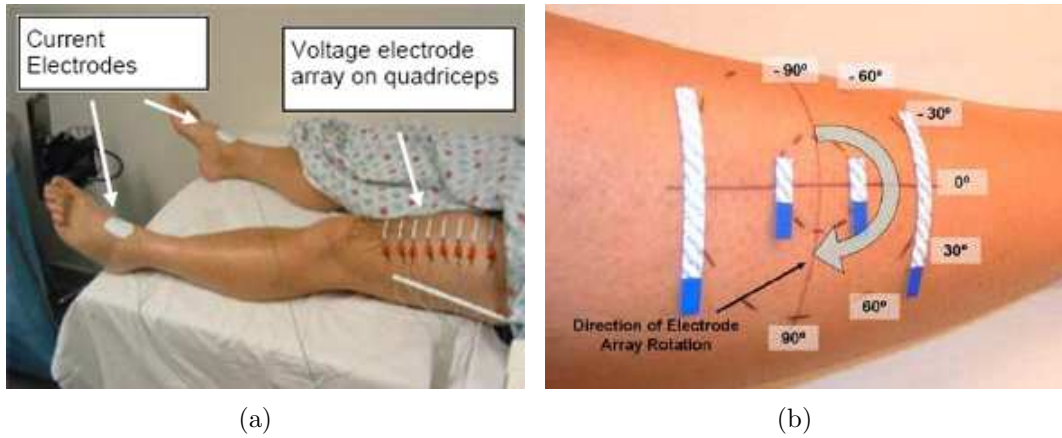


Figure 1-1: A Comparison of linear (a) and rotational (b) electrical impedance myography measurements being performed on a patient.

## 1.4 Concept of Electrical Impedance Myography

Electrical impedance myography is a means of probing the bulk properties and composition of a muscle. Its primary advantages are that it allows a doctor to gather this information non-invasively, without exploratory surgery, and that it provides quantitative results. Rutkove et al. have shown that electrical impedance myography can be used as a robust and quantitative measure of disease progression in a patient, and results may be compared between multiple patients [8, 18].

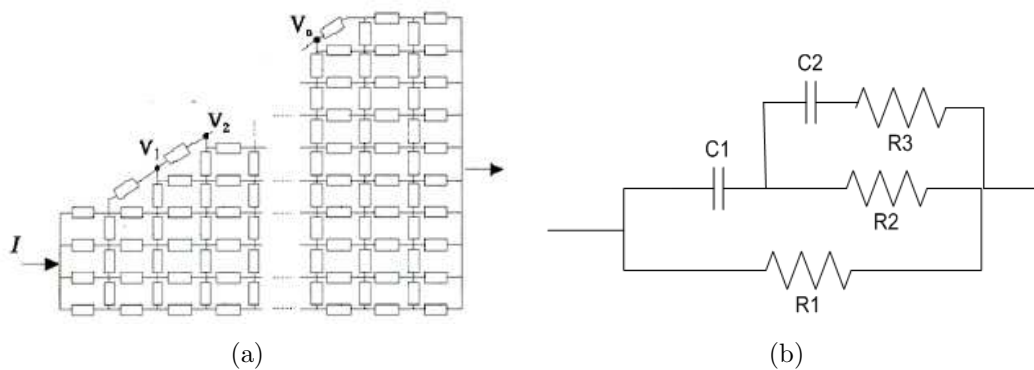


Figure 1-2: A network model of muscle (a), and the corresponding myocyte model (b), present in each box of the network model. (a) was used with permission from the unpublished work of S. Rutkove.

In order to develop the theory of electrical impedance myography, a circuit model

of muscle tissue was developed by Aaron and Shiffman (shown in Figure 1-2). This model has been shown to match measured results. Muscle can be modeled as a network of modules of the type in Figure 1-2(b) where the five elements modeled are extra-cellular fluid resistivity ( $R_1$ ), cell capacitance ( $C_1$ ), intra-cellular fluid resistivity ( $R_2$ ), organelle capacitance ( $C_2$ ), and organelle resistivity ( $R_3$ ). These parameters are of course lumped for the whole model as a muscle may have millions of cells that comprise it, each of which is slightly different from its neighbors. The muscle itself is composed of many millions of myocytes, modeled by the 5-element circuit mentioned above, that are all interconnected as in Figure 1-2(a). In this figure, each box is a myocyte.

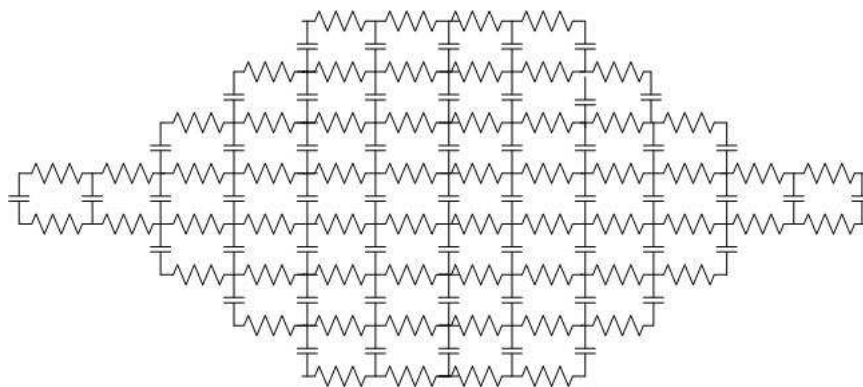


Figure 1-3: Simplified muscle network.

The network can be simplified as seen in Figure 1-3 by dividing the connections into two different types: one type transverse to the muscle fibers, and one type parallel to them [2]. The directions are illustrated on an image of skeletal muscle magnified 200x in Figure 1-4. Current traveling parallel to the muscle fibers is able to flow easily in the extracellular fluid, which surrounds the muscle cells and is comprised mainly of isotonic saline solution, without having to enter the myocytes. This path can be modeled as mostly resistive (the impedances presented by  $C_2$  and  $C_3$  are large compared to  $R_1$ , so current will flow predominantly through  $R_1$ ). On the other hand, current that travels perpendicular to the muscle fibers cannot flow primarily through extracellular fluid and must traverse the myocytes and their cell walls (which have dielectric properties since they are made out of lipids). This path is mostly capaci-

tive because  $R_1$  becomes large. Figure 1-3 captures this simplification by depicting longitudinal current paths as exclusively resistive, and transverse paths as exclusively capacitive.



Figure 1-4: Skeletal muscle magnified 200x.

Drs. Aaron and Shiffman have derived an equation for the impedance of a rectangular network of modules, like the one described above but without  $R_3$  and  $C_2$  which are only significant at higher frequencies. This model is a good approximation to large, flat muscles such as the quadriceps. They have shown that the behavior of the network is similar to that of the individual module, as described in Equation 1.1.

$$Z = \frac{[1 + \omega^2 R_1 (R_1 + R_2) C_1^2] R_1 + \omega R_2^2 C_1 j}{1 + \omega^2 (R_1 + R_2)^2 C_1^2}, \omega = 2\pi f \quad (1.1)$$

One of the most meaningful aspects of the impedance for studying muscle is the phase, defined as the arctangent of the ratio between the imaginary and real parts of the impedance,  $Z$ , according to Equation 1.2.

$$\theta = \arctan \frac{\omega R_2 C_1}{1 + \omega^2 (R_1 + R_2)^2 C_1^2} \quad (1.2)$$

There is usually a peak in the phase at 30-50 kHz, the position and magnitude of which may change during disease progression. Solving for a maximum of the imaginary part (and hence phase) of the impedance yields a peak in the same range when using typical

and realistic values for the component values (Equation 1.3) [18].

$$f_{\text{peak}} = \frac{1}{(R_1 + R_2)C_1^2}(\text{Hz}) \quad (1.3)$$

One can imagine that the values of these parameters may change if some of the muscle cells die or are replaced by scar or fat cells, which is what happens in some diseases. These changes are reflected in the measured impedance [18].

Skeletal muscle cells (which are of primary interest in neuromuscular disease) are organized in a very regular structure consisting of many parallel fibers. The structure is similar to that of wood. As such, there is a large degree of anisotropy in the impedance measurements. This anisotropy can be characterized by taking measurements at different angles relative to the muscle fiber. The differences can be measured by placing electrodes at different angles relative to the grain of the muscle cells. In normal muscle cells there is a large degree of anisotropy since electricity can pass along the muscle fibers by moving mostly through the resistive extracellular fluid, whereas to go transverse to the grain of the muscle electricity will have to pass through the more capacitive cell walls. In the neuromuscular diseases of interest some muscle cells are replaced by tissue that is more homogeneous and does not exhibit as much anisotropy, such as scar or fat cells. The degree of anisotropy can be recorded with rotational electrical impedance myography and used as a measure of disease progression [1].

## 1.5 Goals and Organization of this Work

The primary goal of the project discussed in this work is focused on producing a prototype for easily performing rotational electrical impedance myography. Additionally, we have tried to make our design capable of doing measurements fast enough to perform dynamic electrical impedance myography as well, with the end goal of being able to perform the hybrid dynamic-rotational electrical impedance myography, and be able to see how the muscle changes in real time as it is being used. The combi-

nation of the rotational and dynamic methods has never been used before, but the potential for interesting applications of the combined methods is great. Specifically, the focus has been on developing a fast impedance measurement technique and a handheld electrode probe capable of making rotational EIM measurements.

The rest of this document will be divided into two main parts. Chapter 2 will focus on our techniques for measuring impedance. It will discuss the equipment, circuits, and methods that we are using to measure impedance, as well as compare them to the system currently being used for clinical testing at Beth Israel Deaconess Hospital by Dr. Rutkove. This chapter will also discuss the characteristics of the signal used to stimulate the material to be tested and review the performance achieved.

Chapter 3 will focus on the development of a handheld electrode probe. It will discuss the testing methods developed for evaluating prototypes, as well as the progression of prototypes in the process of arriving at the final design. The final design for the electrode probe will also be discussed in depth, with details about the hardware and software components. In addition, the performance of the electrode probe will be evaluated and compared to traditional electrode measurements.

Concerns for patient safety are the subject of Chapter 4. Finally, Chapter 5 will conclude with an overview of and reflections on this project, as well as possible future directions for this work.



## Chapter 2

# Impedance Measurement

A system capable of performing multi-frequency anisotropy measurements has been built and used at Beth Israel Deaconess Hospital by Drs. Aaron and Shiffman [8], however it is in a state only suitable for research studies and not for mainstream use. The current system is slow, bulky, and requires a trained technician to gather reliable data (Figure 2-1).

The difficulties of the system currently being used in clinical studies stem from two main sources. First, a lock-in amplifier is used to measure each frequency, one by one. If fine frequency resolution is desired, almost one minute is required to make a complete frequency sweep. The long time makes it impossible to measure the dynamics of muscle as it is very difficult for patients to keep a muscle flexed with constant tension for that long. The lock-in amplifier is also very large and expensive, and generally a much more sensitive piece of equipment than is required. Lock-in amplifiers are usually used in physics research to measure micro- and nanovolt signals accurately, which are orders of magnitude more sensitive than is needed for this application. Also, even the best lock-in amplifiers are limited in their bandwidth and are expensive, costing tens of thousands of dollars. The one currently being used at Beth Israel Deaconess Medical Center is limited to 2 MHz, which is below some feature points of interest that are predicted by the 5-element muscle model described in Section 1.4. Due to the lower sensitivity and resolution needed for electrical impedance myography when compared to techniques such as electrical impedance tomography (EIT), or the stan-

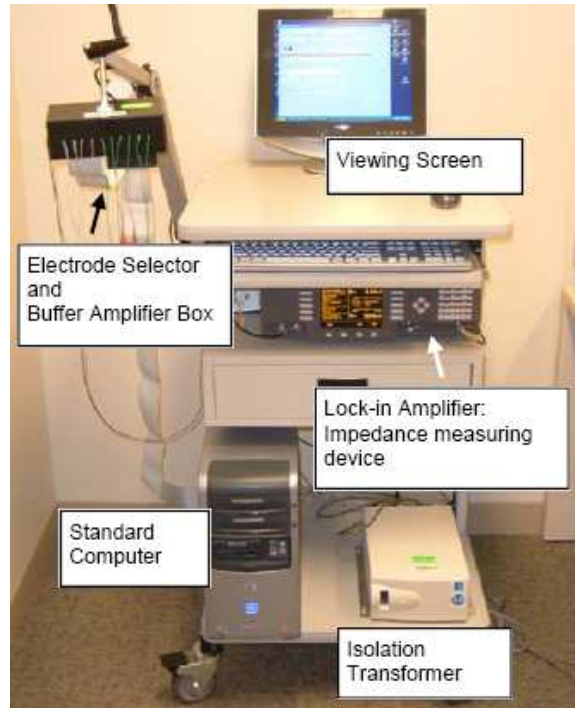


Figure 2-1: Electrical impedance myography instrument currently being used at Beth Israel Deaconess Hospital

dards most laboratory equipment is built for we can take advantage of this relaxation to focus on speed, portability, and cost.

Electrical impedance myography uses essentially the same techniques as many electrical impedance tomography (EIT) systems to measure impedance. Tetrapolar measurements are made by using separate pairs of current and voltage electrodes. It is important to separate the voltage and current electrodes when measuring layered tissue because around the current electrodes current will have to flow through the high impedance skin and fat layers in order to get to the lower impedance muscle. The inward flowing current will make the voltage at the muscle different from voltage measured over the skin. However, if we assume that the voltage electrodes draw only negligible current, current will flow almost exclusively through muscle in the middle of the test area and cause no voltage drop between the muscle and skin surface (Figure 2-2) [1]. If only one pair of electrodes was used to both inject current and measure the resulting impedance we would measure the compound impedance of skin, fat, and

muscle, reducing the signal-to-noise ratio of the muscle impedance.

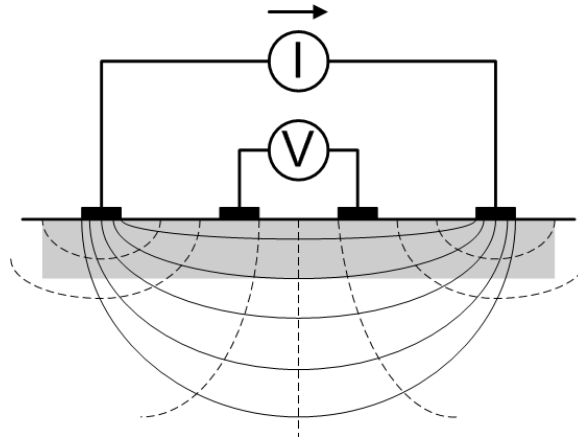


Figure 2-2: Equipotentials (dashed lines) and current flow (solid lines) for a tetrapolar impedance measurement of layered tissue. The shaded region is the skin and fat layer, while the white region is muscle. Adapted from a paper by R. Aaron et al. published in 1997 [1].

## 2.1 Equipment, Circuits, and Methods

Currently, discrete components and lab equipment are being used to make measurements. However, as the project progresses and our methods become finalized, there are plans to create an integrated solution. The signal source being used is a Tektronix model AFG3102 two channel arbitrary function generator (AFG) with 14 bits of amplitude resolution, 100 MHz bandwidth, and a 45,000-sample memory [22]. The signal from the AFG serves as an input for a BJT-based electrode probe driver, the most recent version of which has been constructed using discrete components by Muiyiwa Ogunnika. These components act as a load-independent driver by having high output impedance. A simplified schematic of the driver is in Figure 2-4. The output drives the current electrodes, which are attached to the test area. The voltage is measured and digitized by a Tektronix model TDS3034B four channel oscilloscope. The TD32024B has a 9 bit amplitude resolution (as low as 1 mV, depending on the setting), a bandwidth of 300 MHz, and a 10,000-sample memory (up to a 2.5 GS/s sampling rate) for each of its four channels [21]. Figure 2-3 illustrates the connections

and flow of information in this setup.

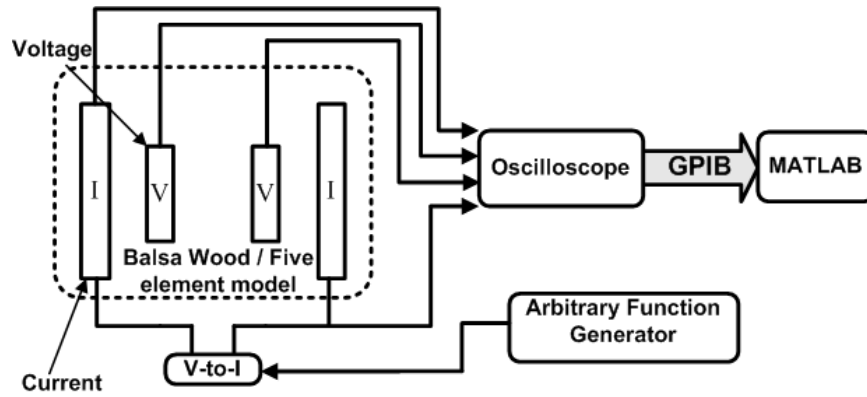


Figure 2-3: System diagram of the prototype measurement setup

The electrode probe driver is designed to inject a differential current into the load. The differential nature of the driver is chosen specifically to eliminate common-mode voltage on the load. This will allow the rest of the circuitry to be much simpler as it will not need as much common-mode rejection capability.

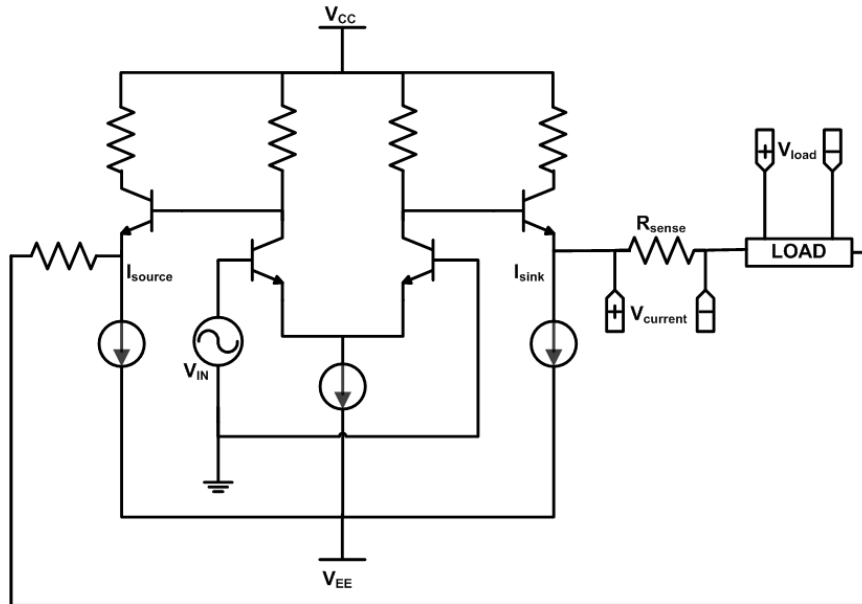


Figure 2-4: Schematic of the electrode probe driver.

Although the voltage going through the load is set to a known value with the AFG and electrode probe driver, the exact value of the current reaching the load

remains unknown because of the unknown load, as well as for reasons like noise, parasitic leakage, and the frequency characteristics of the driver. Since we cannot predetermine the exact value of the current we use a current sense resistor ( $R_{\text{sense}}$  in Figure 2-4) that is in series with the load. The voltage across that resistor ( $V_{\text{sense}}$ ) is measured at the same time as the voltage across the voltage electrodes on the load ( $V_{\text{load}}$ ), and thus we are able to find an accurate impedance. Each terminal is measured by a single-ended channel on the oscilloscope, with all four of the channels sharing a common ground.

A 10,000-sample snapshot is taken of all four channels at once by the oscilloscope at 10 MS/s. The oscilloscope is triggered by an external signal from the AFG once every repetition. The snapshot captures 1 ms, or exactly one period of the repeated waveform, and multiple consecutive snapshots are averaged together, point by point, to cancel out noise and low-frequency oscillations. The noise has many sources including thermal noise, fluorescent light ballasts (many of which operate in the 20 kHz range), and the body's electrical activity. As long as the noise is independent of our input waveform, it can be cancelled out with sufficient averaging. Experiments have been performed to inspect the effect of averaging and find the optimal number of waveforms to average together. Results for 1 to 512 averages were measured and compared, although Figure 2-5 only shows 1 to 16 averages for clarity. One can clearly see that although all of the different cases are close up to 1 MHz, the higher averages are much better at higher frequencies. Also, the lower averages are significantly noisier in the low frequencies than the higher averages. Although there seems to be no loss in accuracy for higher averages, we want to keep averaging to a minimum since it decreases the speed of our system. Averaging more than 16 consecutive snapshots does not seem to improve the measurement significantly and will only reduce the speed of the system, so we have chosen to use 16 averages in the future.

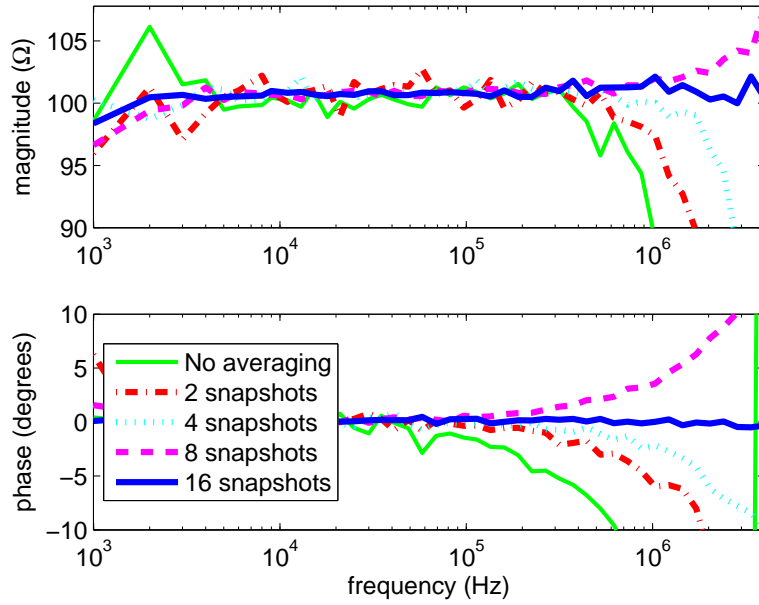


Figure 2-5: Comparison of measurements of a  $100\Omega$  resistor using different amounts of averaging.

## 2.2 Input Waveform

To increase the speed of measurement, we measure all frequencies of interest at once instead of one by one like a lock-in amplifier. This presents us with a decision to make about what kind of composite waveform to use. We would like the waveform to be as broadband as possible, but at the very least it must include frequencies between 1 kHz and 1 MHz. The things that limit us with the laboratory setup are the 100 MHz bandwidth of the arbitrary function generator, and the 10,000-sample memory of the oscilloscope. The relationship between frequency resolution ( $\Delta f$ ), sampling frequency ( $f_s$ ), and number of samples ( $N$ ) for a discrete Fourier transform is illustrated in Equation 2.1.

$$\Delta f = \frac{2f_s}{N} \quad (2.1)$$

The bandwidth ( $f_{\max}$ ) is also related to the sampling frequency by the Nyquist-Shannon sampling theorem, shown in Equation 2.2.

$$f_{\max} = \frac{f_s}{2} \quad (2.2)$$

Thus, if we want to differentiate frequencies of at least 1 kHz we must use a sampling rate of 10 MS/s, and will have a bandwidth of 5 MHz. To ensure that there is no aliasing in case the clocks of the oscilloscope and arbitrary waveform generator are not matched it was decided that the maximum frequency should be limited to 4 MHz instead of pushing the Nyquist frequency. The maximum frequency could have been pushed closer to 5 MHz, but we were already seeing the effects of parasitics at 4 MHz, so we saw no advantage to increasing the maximum frequency.

### 2.2.1 Waveform Type

From the above calculations it was decided to use frequencies between 1kHz and 4MHz. The question now was which of those frequencies to use. The following input signals were considered:

**Impulse or pulse** Ideally, an impulse could be used, but due to the limited bandwidth, the closest option would be a pulse in square, Gaussian, or some other form. The problem with these is that higher frequencies have smaller amplitude.

**White noise** Although white noise should have equal amplitude at all frequencies, this is only true for an infinitely long signal. Also, there would be current at frequencies that are not measured that is needlessly applied to the patient.

**Sinc** This would allow us to control the maximum frequency and would have a flat spectrum like white noise but be more deterministic. However, once again there would be current at frequencies which we are not interested in.

**Sum of sine waves** This method will allow us control exactly which frequencies to use, thus making sure that no unneeded signal power is given to the patient. We can also control the amplitudes of the signal at each frequency.

In the end, we chose to use a sum of sine waves approach since it gives us the best control over the waveform.

### 2.2.2 Frequency Spacing

In our measurements, we inject a current signal composed of a sum of 44 frequencies nearly logarithmically spaced between 1 kHz and 4 MHz, an example of which can be seen in Figure 2-6(b). This waveform is repeated end-to-end to produce a continuous signal with a period of 1 ms. The waveform is stored on the arbitrary waveform generator. The frequencies of each sine wave need to be rounded to the nearest 1 kHz (the repetition frequency), hence the *nearly* logarithmic spacing, to make the complete waveform continuous after repetition.

Examples of waveforms composed of linear and logarithmically spaced frequencies can be seen in Figures 2-6(a) and 2-6(b), respectively. Both are scaled to have the same range to minimize quantization noise. In the waveform composed of linearly spaced frequencies, there are many very small values. On the other hand, the values in the waveform composed of logarithmically spaced frequencies are much more evenly distributed, with many fewer very small values. Figure 2-6(c) illustrates the distributions of the waveforms in a histogram. In the linearly spaced frequency case, many of the frequencies are harmonically related and will add up at certain times, leading to a few very high peaks when compared to most of the values. This has been a problem with EIT systems using composite waveforms in the past [14]. The logarithmically spaced frequency case, on the other hand, does not have this problem as few of the frequencies are harmonically related.

There are many problems with using a waveform where the peaks are much higher than the average sample. Since there are so many low amplitude points, we need to be able to represent them accurately. Firstly, we must ensure that these points are above the noise floor. If we increase the overall amplitude of the waveform to the point where all of the low amplitude values are above the noise floor, the much higher peaks will lead to large peak currents which could be above safety limits. Secondly, since the linearly spaced case has many harmonically related frequencies, the amplitude of the

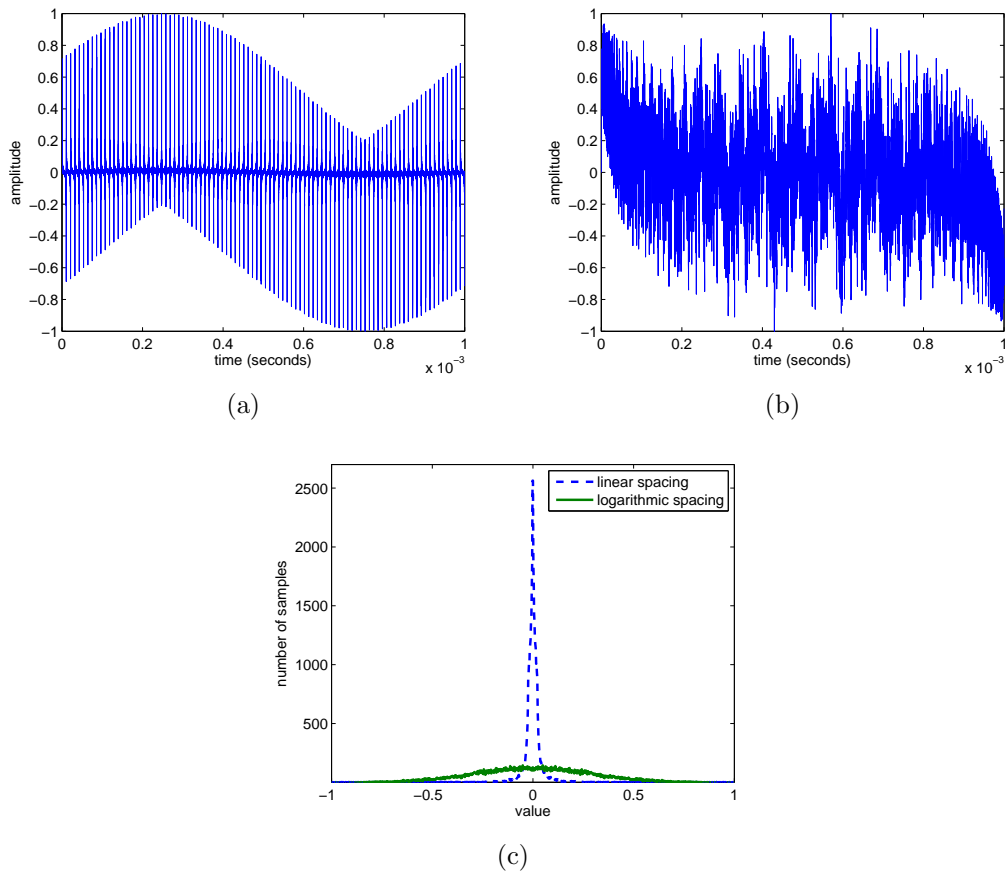


Figure 2-6: A Comparison of composite input waveforms. The waveforms are composed of 44 sine waves between 1kHz and 4MHz at linearly (a) and logarithmically (b) spaced frequencies. The histograms of the samples of (a) and (b) are compared in (c).

input waveform is not a good measure of the amplitude of each frequency component. In fact, after scaling each waveform to have the same range, the frequency components of the logarithmically spaced waveform are almost 2.7 times larger in magnitude than the linearly spaced waveform. This is also reflected in the ratio of their root mean square measures, which is also 2.7.

It seemed clear that using logarithmically spaced frequencies was the better choice. In addition to the difficulties of a linearly spaced frequencies discussed above, the impedance of most circuits varies on a logarithmic scale with respect to frequency (think of Bode plots which always have the frequency plotted logarithmically). By using logarithmically spaced frequencies we can have a finer frequency resolution at lower frequencies where impedance usually varies more quickly and a lower frequency resolution at higher frequency when good frequency resolution is not needed anyway.

## 2.3 Performance

To measure how well our system performed it was first tested on two test circuits. Circuits were used instead of balsa wood or another surrogate material for human tissue because we can accurately model the circuit to get a sense of how closely our measurements match. The two test circuits used were a  $100\Omega$  resistor and a 5-element muscle model as described in Section 1.4 and illustrated in Figure 1-2(b). The values of the components in the five-element model can be seen in Table 2.1.

Parameter	Value
$R_1$	$22.3\Omega$
$R_2$	$121.9\Omega$
$R_3$	$150.6\Omega$
$C_1$	$49\text{nF}$
$C_2$	$1.5\text{nF}$

Table 2.1: Parameters for the 5-element muscle model circuit used in testing.

The impedance measured for the  $100\Omega$  resistor was very close to ideal. Figure 2-5 in Section 2.2 shows measurements of the resistor with different amounts of averaging,

but only the best result, averaging 16 snapshots, has been used since that experiment. The results for a five element muscle model were not as impressive, but still very close to the calculated impedance. The measured phase, in Figure 2-7, starts to deviate from the calculated value significantly at around 1 MHz, but stays very close to ideal at lower frequencies.

### 2.3.1 Sources of Error

The phase deviation seen in the measurement of the five-element muscle model is most likely due to parasitics. Parasitics are inherent imperfections of any real world electronic component. Every wire, resistor, capacitor, and inductor is actually a combination of all of those components with one of them dominating [3].

In our case, we see a phase deviation in the positive direction, suggesting a primarily inductive source of error. Although the error seems to be dominated by inductive effects, it does not mean that only inductive parasitics exist in the system; parasitic capacitances are sure to exist as well, although at lower levels. The inductance is most likely due to the wiring in the model circuit and electrode probe driver. At first, it may seem alarmingly inconsistent that there is much more phase error in the muscle model measurements than in the resistor measurements, but it can be explained by the different values of impedance and constant parasitic impedance. The relatively large value of the resistor overwhelms the wire inductance to the point which it is barely noticeable. However, since the impedance of the muscle model circuit is almost six times smaller at 1MHz than the resistor ( $17\Omega$  compared to  $100\Omega$ ), the inductive effects are much more noticeable.

To illustrate this principle, let us assume that all parasitics are independent of the load and that other than parasitics our measurement of the  $100\Omega$  resistor was perfect. If we also assume that all of the parasitic degradation is due to wire inductance, we can say that the total measured impedance is  $100 + jL_p$ , where  $L_p$  is the parasitic inductance. We can thus isolate the inductance of the system by taking the imaginary component of the measured impedance. Now, let us compare the phase of the muscle model to measurements with the same amount of parasitics. In one case, the model is

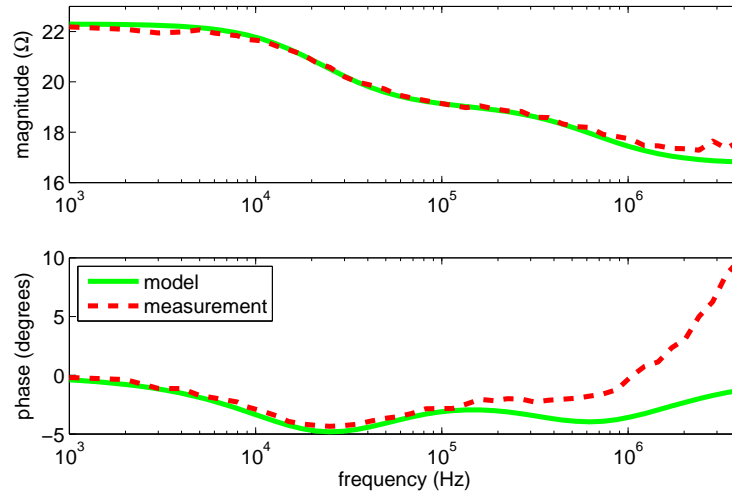


Figure 2-7: Comparison of the ideal and measured impedance of a five element muscle model with the parameters in Table 2.1

as described in Table 2.1, but in the other, the impedance is multiplied by six to put its magnitude around  $100\Omega$ . In Figure 2-8(a) one can see how much closer the phase is to ideal, and in Figure 2-8(b) one can see that the deviation of the phase from ideal becomes around as much as is seen in the measurements of the resistor. In fact, the reactance (the imaginary part of impedance) error in the resistor and 5-element tests are very similar.

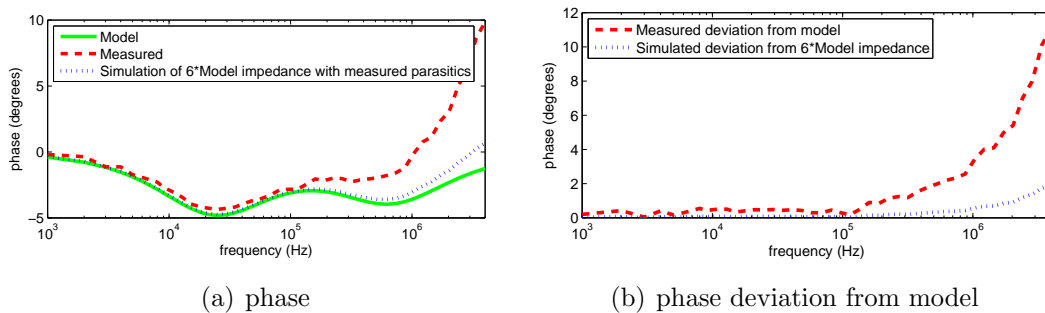


Figure 2-8: The effect of impedance magnitude on the perception of parasitics

Since the impedance of human tissue will be close to that of the five element muscle model, the deviation of measured phase from its actual value can be significant at higher frequencies. However, although this may be a problem now the effects

of parasitics will be greatly reduced as the system gets more integrated. In addition, impedance compensation techniques may be used to effectively cancel out the predetermined parasitic impedance from a measurement. There exist analog circuit techniques for reducing parasitic effects [3], but they often complicate circuitry. Another option could be to do it digitally. As part of a calibration one could measure the impedance of a short circuit, and then subtract that impedance out of later measurements. Although this technique has not been attempted in our system as of the writing of this thesis, it may be tried as part of the group's future work.



# Chapter 3

## Electrode Probe Design

There are many challenges in designing an electrode probe well suited for electrical impedance myography. Designing for *rotational* electrical impedance myography only complicates the problem. In order to be able to take meaningful measurements, the electrode probe must be able to inject current through layers of skin and fat tissues, and measure only the voltage developed across the muscle with as little contribution from the skin and fat layers as possible. Usability is also an important issue. It must be easy to take measurements and get reliable data that is independent of the user for electrical impedance myography to become widely accepted in the medical community. Finally, the electrode probe must be able to measure multiple angles quickly and easily in order for it to be usable for rotational and dynamic electrical impedance myography.

In the electrical impedance myography system used at Beth Israel Deaconess Hospital (Figure 2-1) strip electrodes are being used to make measurements as in Figures 1-1(a) and 1-1(b). The electrodes are placed by hand, making the measurements prone to slight errors based on the electrode positions. Another problem is that only one angle can be measured with each electrode application, making complete anisotropy measurements a lengthy process.

A few alternative electrode systems have been attempted. A mechanical system with four electrodes (two for current and two for voltage) attached to a rotating rod was made as described in [1]. Although this system was able to standardize

the placement of electrodes, the exact placement of the rod was up to the operator making the measurements hard to reproduce.

### 3.1 Testing Methods

As the electrode array being designed is meant to be used on human patients, human testing must eventually be done to prove the device's efficacy. However, before human testing can be done the safety of the device must be proven, and a lengthy approval process must be passed with ethics and safety committees. Since it would be difficult to perform tests on human beings, a proper surrogate material was needed to verify the design of the new electrode array. As one of the main goals of this project is to be able to measure the anisotropy of muscle easily, the surrogate material needed to exhibit anisotropy itself. Also, there needed to be a way of confirming that the electrode array worked and was accurate. This could be done by either obtaining a good model of the surrogate material, or comparing the measurements obtained with the electrode array to those obtained using some other method known to work well.

A few surrogate materials were considered, including flank steak (beef), circuit models, rats, and saline soaked balsa wood. Since the ability to perform tests in an electronics lab would make development of the device easier, circuit models and balsa wood were chosen. Rats and flank steak are good materials in the sense that they will likely exhibit impedance similar to human muscle, but they are both hard to preserve and rats would also require a lengthy approval process. A circuit like the five element myocyte model discussed in Section 1.4 and a resistor were used to test the electronics and ensure that results were matching the expected impedance, but it could not be used to test the electrode array fully. Although a network of circuits could have been used to test an electrode array, it would be difficult to construct. The scale of the network constructible in the laboratory would be many orders of magnitude smaller than any biological material (which may have millions of myocytes). In order to test the electrode array, saline soaked balsa wood was used, as it exhibits anisotropic characteristics similar to human muscle [5], and is flat so that the electrodes may be

applied easily. To verify the validity of the measurements made using the electrode probe, they were compared to measurements made using adhesive strip electrodes as described in [5].

Although balsa wood is a much more controlled medium than beef or human tissue in the long run, significant drying can occur quickly. The drying affects the values of measurements made several minutes apart, especially the magnitude. Similarly, it is difficult to ensure the same level of saline saturation between measurements. Chin et al. have shown that the impedance of balsa wood begins to settle after a few weeks of soaking, but small fluctuations still occur as it is removed and put back in a saline bath [5]. Due to this problem, we try not to concern ourselves with small differences in impedance magnitude unless the measurements are taken very close together in time. Instead, we pay more attention to relative measurements such as phase or the location of extrema in frequency.

## 3.2 Electrode Probe Prototypes

The first idea for an electrode array capable of making rotational measurements was to attempt something similar to the design described in [1] with strip electrodes connected to a rotating rod. The design was to call for automating the rotation with a motor in order to remove human error and standardize measurements. This idea was not pursued past the design phase as it was deemed to be too mechanically complex. In addition, although the angular resolution of this design would be very high, the need to physically rotate the electrodes would make measurements too slow for dynamic, rotational electrical impedance myography.

The next idea was to superimpose the strip electrodes from each angle onto one electrode probe (Figure 3-1), and then select groups of electrodes to use for each angle using relays or solid-state switches. It was impossible to achieve both high angular resolution and small electrode probe size. Since each set of electrodes uses a portion of the available circumference of the electrode probe and the electrode strips cannot overlap, adding more angles would reduce the maximum size of the electrodes. The

circumference can be increased by making the diameter of the electrode probe larger, but that makes it unusable for small muscles. Reducing the size of the electrodes can also increase angular resolution, but the research of Rutkove, et al. has shown that larger current electrodes produce better anisotropy at frequencies above 100 kHz in a currently unpublished work.

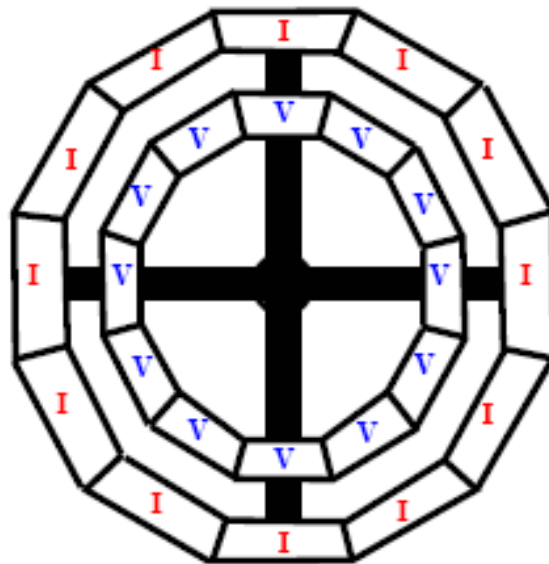


Figure 3-1: An early electrode array design: superposition of electrode strips.

### 3.2.1 Electrode Arrays

The angular resolution of the electrode probe could to increase greatly if it were possible to overlap the larger current electrodes. Although this is unattainable with solid strip electrodes, it is possible to do this in a sense by connecting together smaller electrode cells into larger “virtual” electrodes, with some of the cells being used for more than one virtual electrode. One can imagine an electrode probe made up of a matrix of small electrodes (we will call them “cells”), just like a computer monitor is made up of pixels, where each cell can be connected to any other. With this design one can “draw” current or voltage electrodes in any arbitrary shape or position (given a high enough resolution of the cells), while leaving the rest of the cells unconnected.

An example configuration can be seen in Figure 3-2. Although at the limit of infinite resolution the virtual electrodes become equivalent to actual strips, this analogy breaks down as the resolution decreases, and thus the spacing between cells increases.

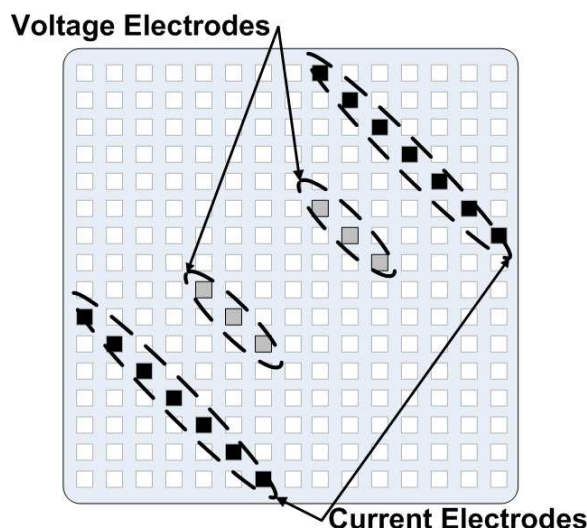


Figure 3-2: Concept of electrode array with virtual electrodes “drawn” on.

Although using a matrix of electrodes for this purpose has not been attempted to date, studies of the interaction of small arrays of electrodes with biological tissues have been done. Specifically, Leonid Livshitz et al. [12] have presented mathematical models confirmed with experiments that describe the general behavior of potential and current density distributions in layered biological tissue consisting of skin, fat, muscle, and bone layers. They have discussed the changes depending on the size and configuration of the electrodes in the array. Although their studies were concerned with muscle stimulation, muscle fatigue and higher currents than are of interest to us (1mA compared to 100mA), the results are still very valuable.

The study shows that a uniform current density distribution is achievable at the fat-muscle interface using multiple electrodes. In fact, it is shown that the current density distribution using multiple electrodes can be more uniform than using one electrode of the combined area. By spreading out the current electrodes over a larger area the peak current density is reduced on the surface of the skin while the current in the middle of the test area remains the same. Increasing the space between the

positive and negative electrodes increases the flatness of current distribution, thus a proper distance between the current and voltage electrodes must be found taking into account the total size of the electrode probe and the spacing between voltage electrodes (which influences the number of measurable angles).

The results of the study were important for this project in that it provides a basis of using multiple electrodes to simulate a larger current electrode, but there is still the question of whether using multiple voltage sensing electrodes would be equivalent to using one larger one. Since the voltage electrodes would have a very high impedance (in the  $M\Omega$ ) negligible current will flow through them. The effect of this will be to keep the tissue's potential distribution unchanged whether or not there are voltage electrodes attached to the skin. By using multiple electrodes connected together, the voltage at the node of their common connection will just be the average of the voltages at each of them. Since our design will strive to place the voltage electrodes over a region of flat current density, the voltage at each electrode should be the same, and thus so should their average. The circuit itself can be thought of as a passive averager (Figure 3-3). If all of the resistances are equal (a valid assumption since the variations in contact impedance will be small compared to the input impedance of an amplifier used to detect the measured voltage), Equation 3.1 reduces to  $V_{\text{avg}} = \frac{V_1+V_2+V_3}{3}$ .

$$V_{\text{avg}} = \frac{V_1/R_1 + V_2/R_2 + V_3/R_3}{1/R_1 + 1/R_2 + 1/R_3} \quad (3.1)$$

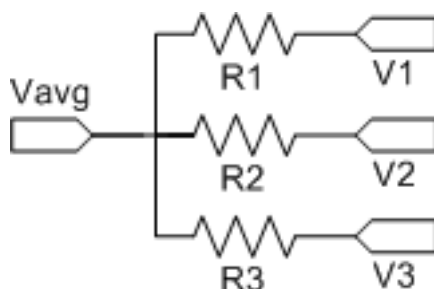


Figure 3-3: A passive averager circuit.

### 3.2.2 Prototype Design

A few electrode probe prototypes were built to test the above claims. The prototypes were meant to test the reliability of using interconnected electrode cells to replace a larger single electrode. Two different designs were constructed to test different cell configurations and sizes in the form of a rectangular grid (Figure 3-4). The prototypes were constructed using 1/8" clear and rigid acrylic plastic cut using a CAM laser cutter. The CAD models were made using the Rhinoceros<sup>®</sup> 3.0 Nonuniform rational B-spline (NURBS) modeling environment.

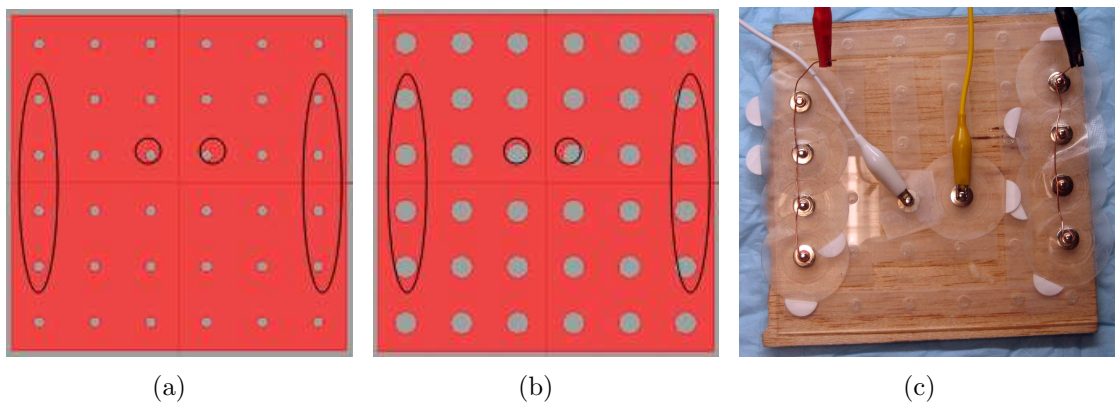


Figure 3-4: Rectangular electrode probe prototypes demonstrating different amounts of the total area being covered by the actual electrode cells: 200mil diameter cells and 3.1% coverage (a), and 400mil diameter cells ad 12.6% coverage. An example setup is shown in (c).

For these prototypes, the cut out circles (200mil in diameter for Figure 3-4(a) and 400mil in diameter for Figure 3-4(b)) were used as wells to hold conductive electrode gel capped with standard silver/silver chloride metal electrodes. The gel was used to make a good electrical connection with the balsa wood that these designs were tested on. During the tests, some of the cells were physically connected together using wire as in Figure 3-4(c).

### 3.2.3 Prototype Results

Measurements from the prototypes were encouraging in that the phase for measurements using electrode strips and the 400mil array matched very well, an example of

which is shown in Figure 3-5. However, the magnitude of the measured voltage is significantly lower for the prototype than the strips. Although the exact reason for this discrepancy is unknown, it may be due to the comparative width of the cells and strips. The strips are only 190mils wide, so even if the strip's and cell's centers were the same distance apart the edge of the electrode cells would only be at 80% the distance of the strips. Another reason for the difference in magnitude could be due to the balsa wood being dryer while the electrode strips were used, making it harder for current to move through the wood. For the reasons discussed in Section 3.1, the great match in phase is more important to us than the slight mismatch in magnitude.

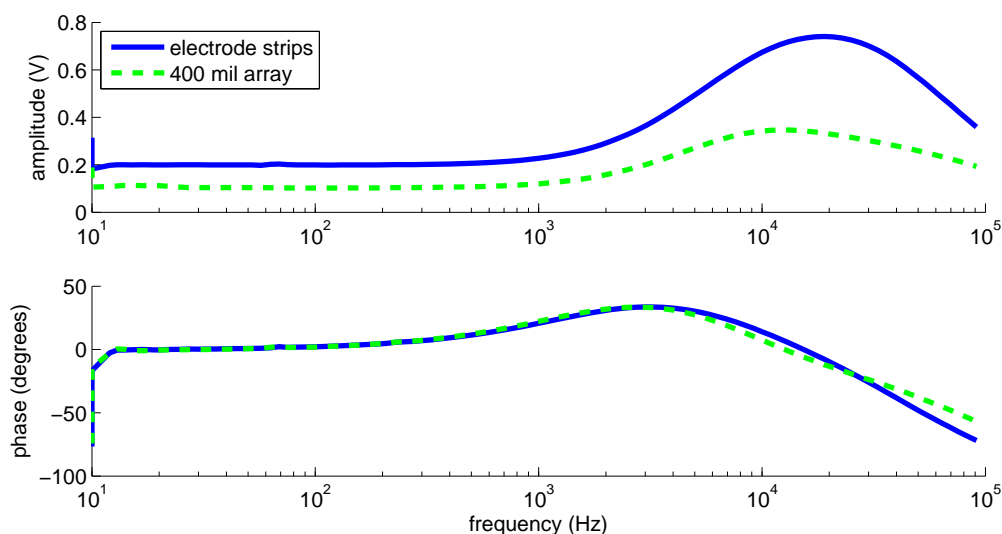


Figure 3-5: A comparison of bode plots of balsa wood as measured using 400mil rectangular prototype and electrode strips.

Another set of experiments that were performed using the prototypes was to test the effect of gel coverage on measured anisotropy. The concern was that as the percentage of the total area that is covered by gel and electrodes increases, there is a greater risk of current shunting across the isotropically conducting testing surface (through the gel, etc.) and not being injected into the anisotropic material we are testing. Three scenarios were tested.

1. Only the cells being used for the measurement at hand would be filled with gel and allowed to contact the wood.

2. All of the cells were filled with electrode gel.
3. A layer of electrode gel was slathered on the wood covering the whole testing surface.

Each consecutive scenario increases the percentage of testing surface covered by conducting gel, and each was tested on both the 200mil and 400mil cell diameter prototypes. As expected, a decrease in anisotropy was observed with increasing gel coverage. Also, less anisotropy was observed with the 400mil prototype than with the 200mil prototype, and the decrease in anisotropy was less profound in the 400mil prototype. All of these results suggest that significant shunting does, in fact, occur across the surface of balsa wood when it is covered with conducting gel. The results are available in Figure 3-6.

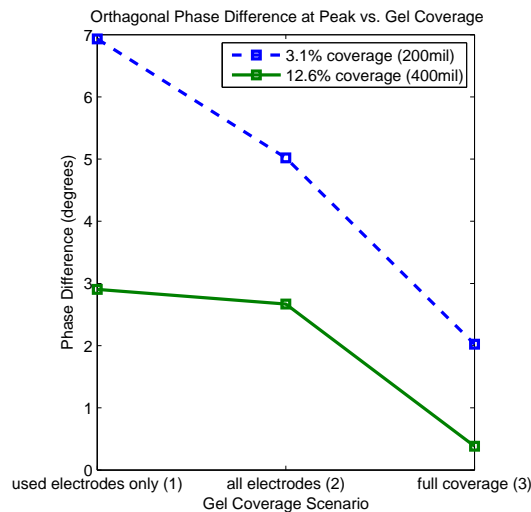


Figure 3-6: The effect of gel coverage on observed anisotropy in balsa wood.

More tests were conducted at Beth Israel Deaconess Hospital on live human tissue by Chin and Rutkove to see if the same effects would occur in layered tissue [15]. However, instead of using electrode gel and the prototype designs, they used electrode strips. To provide a conductive path on the surface of the skin, a large adhesive electrode was put between the voltage electrodes. No difference in anisotropy was seen with or without the central electrode. Although the results were different in this

set of tests, they do not necessarily contradict the results measured on balsa wood due to the different scenarios. The central electrode used was placed just between the voltage electrodes, making the path to it from the current electrodes much higher impedance than the path through a thin layer of skin and fat tissues and then through muscle. Figure 3-7 illustrates the placement of electrodes and the different current paths. From these results it is clear that one would like to keep the testing surface free of any conducting materials, but that having a small part of it covered with such a material would be acceptable on layered tissue.

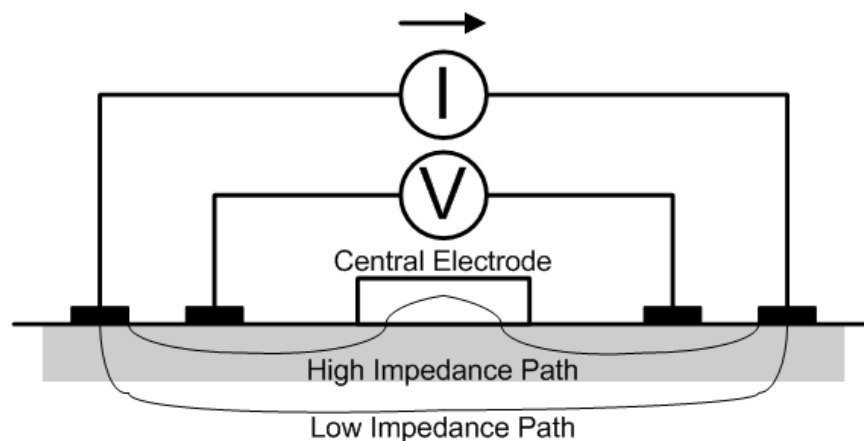


Figure 3-7: An illustration of the current paths through layered tissue after the application of a central electrode. The shaded region is the skin and fat layers, while the white region is muscle.

### 3.3 Final Design

The final design of the electrode probe is based on the electrode array concept presented in Section 3.2.1, and is capable of making tetrapolar impedance measurements as described in Chapter 2. However, unlike the prototypes in 3.2.2, it is extended by increasing electrode density and adding electronics that can selectively connect many electrode cells together. The connections between electrodes are controlled by a PC via a USB interface.

Since electrical impedance myography is still in development, the electrode probe

has been designed to be as modular and flexible as possible so that changes to one or more parts of the system will require minimal changes to the electrode probe. In addition, the electrode probe does not depend on the impedance measurement method used. It simply provides the four terminals needed for a tetrapolar measurement to the rest of the system. The probe has been divided into four modules, which are discussed in detail below. The hardware for the modules was manufactured using two-layer printed circuit board (PCB) technology. A system diagram and photograph of the complete and assembled system can be seen in Figure 3-8.

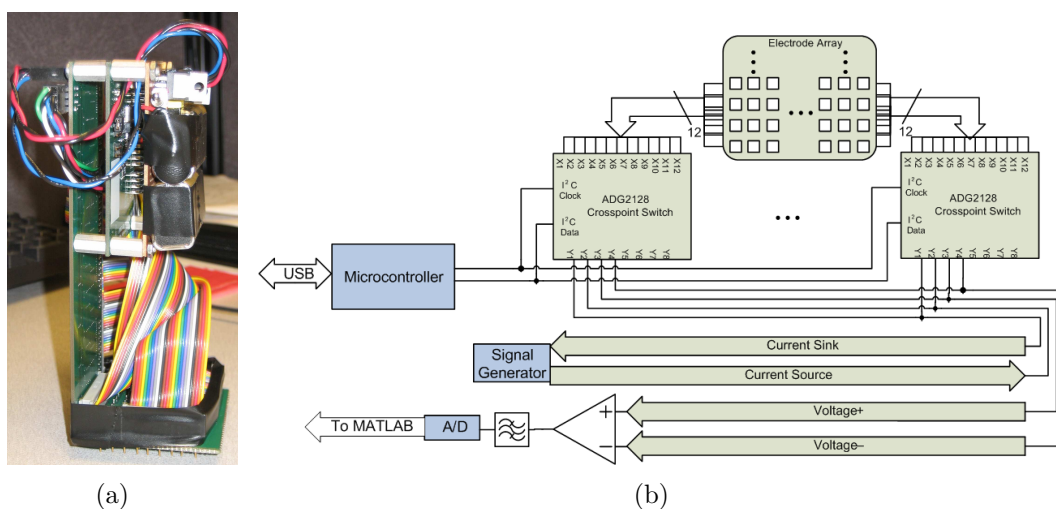


Figure 3-8: Illustrations of the complete electrode probe: a photograph (a), and system diagram (b).

### 3.3.1 Electrode Array

The electrode array is the only thing that actually touches the patient. It consists of many small electrodes cells arranged in a pattern. Due to the modular design of the electrode probe we can have many different electrode arrays, of different sizes and cell configurations, which can be switched in our out. For testing purposes, three different electrode arrays were built, each having 80 cells. Two arrays were built in square configurations, and one with a circular configuration. The square arrays were built in two sizes, one being 3.2” on each side with 0.8” spacing between each

cell and the other being 1.6” on each side with 0.4” spacing between each cell. The circular array has three concentric rings of electrodes with diameters of 1.6”, 0.8”, and 0.4”. The rings have 12, 24, and 48 cells spaced evenly around their circumferences, respectively. Figure 3-9

The different configurations were meant to test the different effects of electrode placement and composition. Some examples of the things that these arrays were designed to test are given below.

- Straight electrodes compared to curved electrodes.
- The effect of cell spacing
- The effect of distance between current and voltage electrodes.

Although some of the above things have already been tested as described in Section 3.2.3, the electrode arrays can be used to perform more precise and complete tests quickly and easily.

The electrode arrays, like the rest of the modules, were manufactured as rigid printed circuit boards. The rigid nature of the arrays was chosen at the advice of Dr. Rutkove because of the ease of manufacturing compared to flexible printed circuit boards and because they could be used to compress the muscle and get more robust readings. Vias were drilled into the board to which gold plated pins were soldered to create the electrode cells (examples can be seen in Figure 3-9).

The pins proved to work well on balsa wood as they could be inserted slightly into the wood to provide a good electrical connection, but they are too uncomfortable for prolonged human use. Future versions of the electrode arrays will experiment with designs that substitute pins for metal pads which are flush to the board’s surface. The wide range of materials available as plating finishes for pads, including gold, silver, and organic coatings, will allow us to further optimize the design.

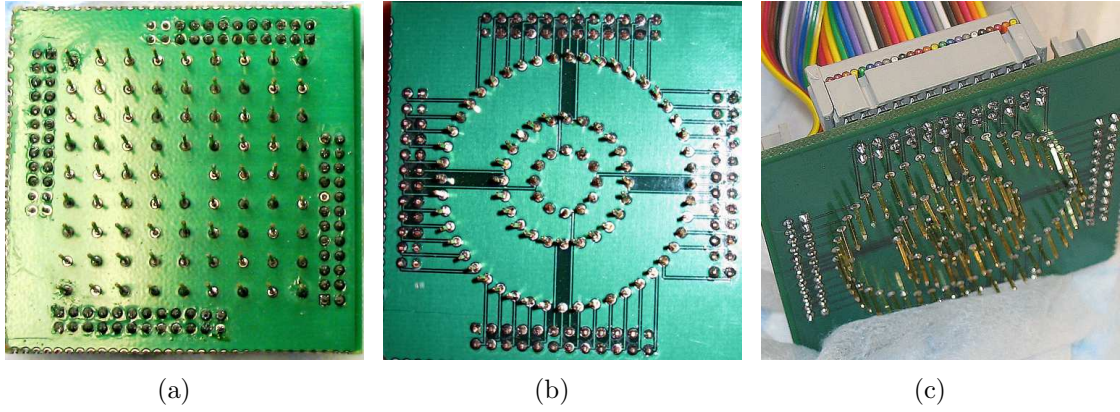


Figure 3-9: Examples of electrode arrays: a square array (a), circular array (b), and side view of the pins used in the circular array (c).

### 3.3.2 Switching

The switching module makes connections between individual cells in the electrode array to form the current and voltage terminals. To allow maximum flexibility in array design, each cell should be able to act as any of the four current or voltage terminals, or stay floating.

After deciding to use the electrode array concept, the first thing that needed to be done to make the design achievable was to find a suitable device capable of connecting many cells together while allowing current to flow both in and out of the cells at the frequencies of interest. Although the setup that is being used at Beth Israel Deaconess Hospital does not have an electrode array, it has the capability of making measurements at a small amount of electrodes. This is accomplished by using a bank of electromechanical relays. Although relays have a high bandwidth, allow bidirectional current flow, and have excellent electronic isolation, they are very large and slow. Their size and weight would make a handheld probe impractical and expensive. Since each cell should be able to connect to any of the four measurement terminals, as well as float without any connection, even a low resolution array of 5x5 cells would require at least 100 relays, which would be unmanageable.

The large amount of identical devices led to the idea of using an integrated solid-state solution. An analog switch is a device that behaves like a relay, but with no

moving parts. Instead, one or a pair of MOSFETs are used and can be switched from high resistance to low resistance depending on a digital input signal. Analog switches are faster and much smaller than relays (typically available in integrated packages of multiple switches), but do have some drawbacks. Compared to relays, they have less electrical isolation between the analog side and digital side. Also, being made of MOSFETs, analog switches are active devices. As such, the analog signal is limited in maximum current and voltage swing by its power rails. However, most of these disadvantages are for high power applications which electrical impedance myography is not. In fact, most devices are used for video or telecommunications applications which typically operate in the 100s of MHz and around 10 volts; both of these specifications are about an order of magnitude higher than what is needed for electrical impedance myography.

### **Crosspoint Switches**

An Analog Devices model ADG2128 crosspoint switch was finally chosen for the electrode probe. The ADG2128 was chosen because of its high density and simple programming interface. Being a crosspoint switch, it can connect any of its 12 inputs to any of its 8 outputs, making an electrode array with 100 or more electrode cells feasible. The device has a 300 MHz bandwidth, and is capable of handling a  $\pm 3V$  input swing relative to analog ground [4]. These specifications are sufficient for our application.

The ADG2128 is controlled by an I<sup>2</sup>C serial interface. I<sup>2</sup>C is a two line serial computer bus that is meant for communication between multiple low speed components. Each device must have an address and can share the same two line bus, which makes routing many components together easy and requires little board area. This compact bus is a key advantage for this application because we will have to use many crosspoint switches together to control a high resolution electrode array. Communication of up to 3.4 Mbit/s is achievable with modern I<sup>2</sup>C, but only 400 kbit/s (fast enough to allow many electrode reconfigurations per second) is used in this project. The ADG2128 allows the user to set only the lowest 3 bits of the chip's 7-bit I<sup>2</sup>C ad-

dress. This limits us to at most 8 chips on a single bus, and thus at most 96 electrode cells ( $12 \text{ inputs} \times 8 \text{ chips}$ ). However, this can be extended by using separate busses for groups of eight chips; this method is discussed in more detail in Section 3.3.3.

## Circuit Board

The design of the switching module circuit board was not trivial. The board had to be very dense in order to fit all of the connections for eight crosspoint switches (for up to 96 electrode cells) in a handheld package. This board also features a separation between the analog and digital side of the system. The ADG2128 crosspoint switch uses both digital and analog circuitry, which should be kept separate to keep the analog signals free of noise from the digital side. To do this, there are separate ground planes, and each side is contained in a separate part of the board. Another threat to signal integrity is stray capacitance between the measurement terminals [3]. To reduce this effect, a well connected ground strip is placed between each terminal to act as a guard plate. A photograph of the switching module board is in Figure 3-10

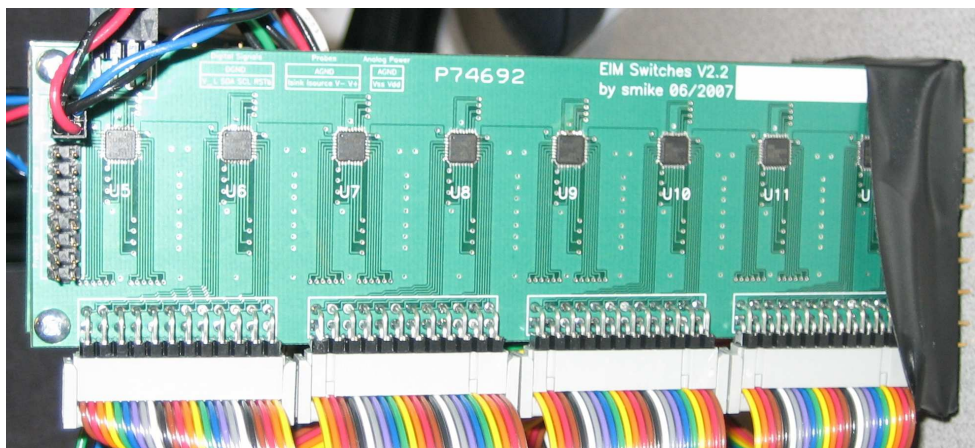


Figure 3-10: A photograph of the switching module circuit board.

Since we only need four terminals to take a tetrapolar measurement and the ADG2128 has eight outputs, the switching board has been made capable of taking two simultaneous tetrapolar measurements. This feature is meant to be used in future experiments of simultaneous multi-angular measurements discussed further in

Section 5.1. Simultaneous multi-angular measurements have the potential of reducing the time it takes to take a full rotational measurement, and thus improve temporal resolution for dynamic electrical impedance myography.

### Using Multiple Switching Modules in Parallel

Although 96 electrode cells have been enough to make electrode arrays with sufficient resolution to perform preliminary testing, higher density arrays are envisioned for the future. The addressing scheme of the ADG2128 limits the number of electrode cells that can be connected to one board, as discussed above. To allow for more electrode cells, an address extension scheme has been developed (as described in Section 3.3.3) to enable the use of up to four switching modules in parallel, and thus up to 384 electrode cells in one electrode array.

The Switching modules are designed to be stackable in a way that connects the two sets of four measurement terminals, as well as the analog power rails. The only connections that need to be different to each module are the digital control signals and inputs from the electrode array. Since all of the analog signals are connected through stacking, the whole stack of switching modules acts like one larger module. Figure 3-11 shows two modules stacked together.

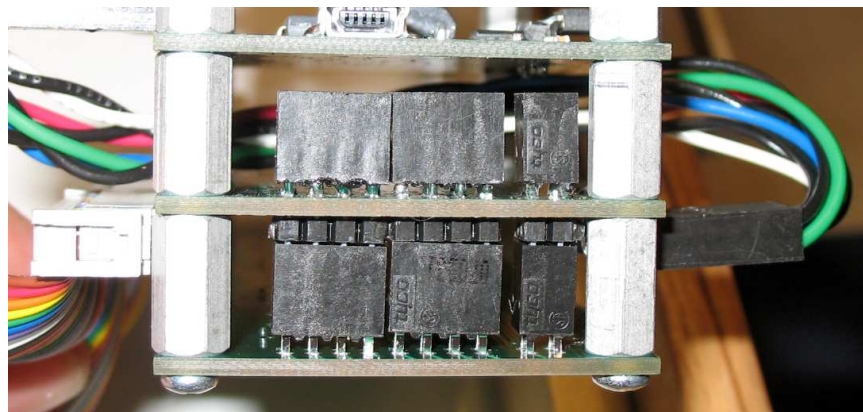


Figure 3-11: A photograph of the analog terminals of two switching modules stacked together.

### 3.3.3 Controller

The controller interfaces the PC to the electrode probe. It interprets commands coming from the PC and tells the switching module which connections to make. It can also tell the PC operator the status of connections. The controller module contains a microcontroller, digital power supply (described further in Section 3.3.4, demultiplexer, and connections for the digital control busses for up to four switching modules. The busses consist of I<sup>2</sup>C data and clock signals, a reset signal, and digital power. A picture and system diagram of the module can be seen in Figure 3-12.

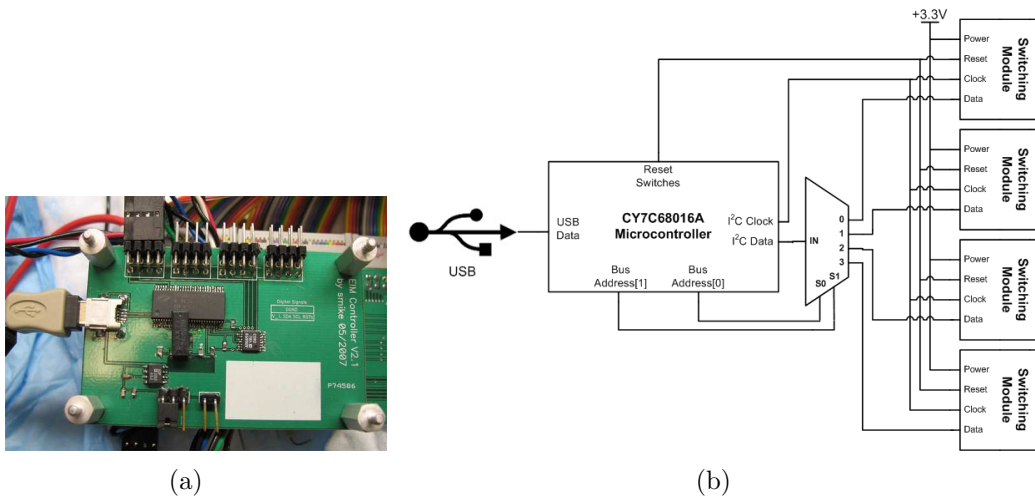


Figure 3-12: A photograph (a), and a system diagram (b) of the controller module.

#### Microcontroller

A Cypress Semiconductor CY7C68016A EZ-USB FX2LP microcontroller is used in the electrode probe. The microcontroller has built in support for USB and I<sup>2</sup>C communication, making it ideal for this application. The microcontroller operates at 3.3V, and uses an external crystal to generate a 24 MHz clock [7].

Although it has four 8-bit general I/O ports, only one of them is used. One bit is used to generate a reset signal, which is common to all crosspoint switches, and two more bits are used for address extension as described below.

## I<sup>2</sup>C Address Extension

To increase the number of electrode cells that can be put into an array, we had to extend the addressing scheme of the ADG2128s. The devices are limited to a 3-bit user programmable address, so at most eight chips can be placed on one bus. To remedy this, separate busses are used for groups of eight chips, with up to four busses usable by the electrode probe. This scheme allows the PC-side software to control 32 crosspoint switches seamlessly, and the use of denser electrode arrays.

A 4-port analog demultiplexer is used to route the I<sup>2</sup>C data signal to each bus, while the I<sup>2</sup>C clock, power, reset signals remain common between all of the busses. All of the signals except for the data signals can be shared as the ADG2128s function exclusively as slave devices, and will never initiate communication by themselves. Although the ADG2128s function as slaves to the microcontroller, they may still send back data upon request. For this reason a standard digital demultiplexer cannot be used for the data signal, and an analog one is needed instead. An analog demultiplexer is capable of signals originating at either the output or input, while digital demultiplexers can only transmit signals one way.

### 3.3.4 Power Supplies

There are two separate power supplies in the electrode probe, one for the analog circuitry and the other for the digital control circuitry. The digital circuitry requires +3.3V and originates on the controller module. The controller module is able to produce enough power on-board to run itself and the switching modules. It has been designed to draw power from either the USB bus (at +5V) passed through an Analog Devices model ADP3303 linear voltage regulator, or an off-board source.

The analog power supply is contained on its own board (Figure 3-13) and provides +5V and -5V power rails to the analog side of the ADG2128 crosspoint switches on the switching modules. The voltages are generated by LM7905 (-5V) and LM7805 (+5V) linear voltage regulators connected to two replaceable 9V battery connected in series. This serves to electrically isolate the patient side of device from potentially

dangerous AC line power.

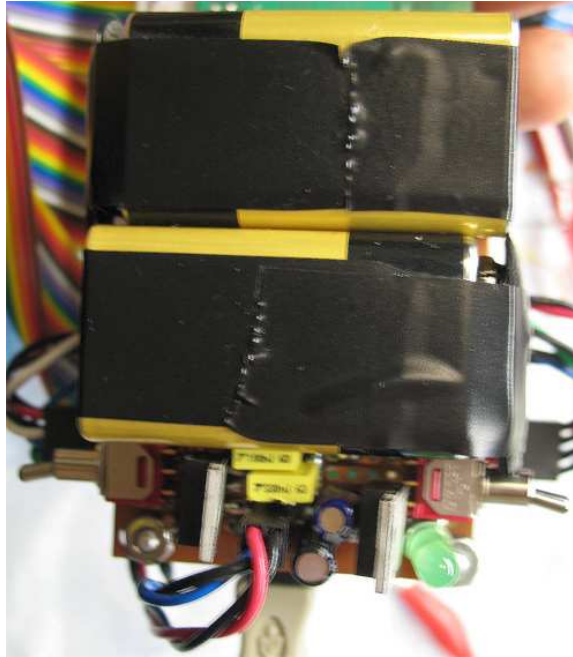


Figure 3-13: A photograph of the analog power supply module.

Unlike the rest of the modules, the analog supply module was constructed by hand on a bread board due to its simplicity. It also has flip switches to turn the supply off, and an LED whose brightness can be used to tell how much voltage is being produced.

### 3.3.5 Software

Custom software and firmware was written for the electrode probe to allow a user to easily reconfigure the electrode probe multiple measurements quickly and easily. The software can be divided into three parts which are highly decoupled, ranging from the low level firmware that resides on the microcontroller, to user-friendly graphical user interfaces. The lower level components were written in the C programming language, and the higher level components were written in Java and use XML to store user settings and probe configurations.

## **Firmware**

The firmware's job is to translate messages from the PC into I<sup>2</sup>C commands for the ADG2128s, and vice versa. It is also responsible for deciding which bus to use for I<sup>2</sup>C communication based on the extended address of an ADG2128 (this is described in more detail in Section 3.3.3). A simple protocol is used to encode these messages, which are sent in variable length packets. There are three different types of commands that can be sent: set the state of a switch, get the state of a switch, or reset all switches to the default "off" position. After each command is completed, an acknowledgement byte is sent back to the host PC. The acknowledgement is required to ensure that commands are not sent faster than the microcontroller can process them, and also helps in debugging the system. The firmware was written in C and a compiler provided by Cypress semiconductor specific to the microcontroller was used.

## **Library and Driver**

A command line tool and dynamically linked library (DLL) were written in C to interface with the firmware. This code provides a way to send commands and receive responses on a PC. The DLL can be imported into user code to create higher-level applications without having to worry about the low-level implementation of the electrode probe. Although the command line tool can be used instead of the DLL in user code as it provides the same functionality, it was designed as a debugging tool. By having human readable input and output for all three basic commands, the command line tool can be used to isolate problems with an electrode probe application.

The PC-side software relies on the Cygwin Linux emulator and "libusb-win32" libraries to access the microcontroller via USB. A lib32-usb based driver has also been made that automatically loads the firmware onto the microcontroller when it is connected.

## Configuration

The higher-level software, including the user interface (discussed in more detail below) relies on three layers of abstraction in order to make the configuration of different electrode probe setups easy and flexible. The configurations, which are specific to an electrode array design, are stored in XML files, examples of which can be seen in Figure 3-14. The first level defines the address of each cell in the array. Since each crosspoint switch has 12 inputs, we can use one id number for a cell address. Thus, a cell with id 26 would refer to input 2 ( $26 \bmod 12$ ) on chip 3 ( $\lceil \frac{26}{12} \rceil$ ). A position is also associated with each cell so that it can be displayed correctly in a rendering of the electrode array. The cell definitions reside in a separate XML file from the other abstraction layers. This is done because this layer creates a physical mapping to the electrode array, whereas the other layers create logically mappings between groups of cells. Once a cell definition file is made, it becomes easy to switch between different electrode array designs. All that is required is to snap the new array into place, and specify its cell definition file in the software.

The second layer of abstraction defines electrodes as sets of cells. Each electrode must have a unique name, often something descriptive. A single cell can be included in multiple electrodes, thus making the “overlapping electrodes” discussed in Sections 3.2 and 3.2.1 a reality. The third, and highest, level of abstraction defines groups of electrodes. Since the goal of electrical impedance myography is to take tetrapolar impedance measurements, it makes sense that one would like to activate a certain group of electrodes together all the time. In addition to logically binding together multiple electrodes, each electrode is assigned an output. Thus, an electrode group definition has all the information needed to make the proper connections in the electrode probe. A name is also associated to each group so that it is easily recognizable by the user. Although this design is geared to making tetrapolar measurements, an electrode group can have any amount of electrodes so that if one is making simultaneous multi-angular measurements, all electrodes can be assigned at once. Both the electrode and electrode group definitions are stored in the same file, which also

has a reference to the associated cell configuration file so that all three abstraction layers can be bound together.

<pre> &lt;cell&gt;   &lt;id&gt;62&lt;/id&gt;   &lt;location&gt;     &lt;x&gt;61&lt;/x&gt;     &lt;y&gt;494&lt;/y&gt;   &lt;/location&gt; &lt;/cell&gt; </pre>	<pre> &lt;electrode&gt;   &lt;name&gt;outer_150&lt;/name&gt;   &lt;cellId&gt;64&lt;/cellId&gt;   &lt;cellId&gt;62&lt;/cellId&gt;   &lt;cellId&gt;94&lt;/cellId&gt;   &lt;cellId&gt;65&lt;/cellId&gt;   &lt;cellId&gt;60&lt;/cellId&gt;   &lt;cellId&gt;61&lt;/cellId&gt;   &lt;cellId&gt;63&lt;/cellId&gt;   &lt;cellId&gt;95&lt;/cellId&gt;   &lt;cellId&gt;93&lt;/cellId&gt; &lt;/electrode&gt; </pre>	<pre> &lt;group&gt;   &lt;name&gt;middle_165&lt;/name&gt;   &lt;electrode&gt;     &lt;name&gt;middle_165&lt;/name&gt;     &lt;output&gt;0&lt;/output&gt;   &lt;/electrode&gt;   &lt;electrode&gt;     &lt;name&gt;middle_345&lt;/name&gt;     &lt;output&gt;1&lt;/output&gt;   &lt;/electrode&gt;   &lt;electrode&gt;     &lt;name&gt;outer_165&lt;/name&gt;     &lt;output&gt;2&lt;/output&gt;   &lt;/electrode&gt;   &lt;electrode&gt;     &lt;name&gt;outer_345&lt;/name&gt;     &lt;output&gt;3&lt;/output&gt;   &lt;/electrode&gt; &lt;/group&gt; </pre>
(a)	(b)	(c)

Figure 3-14: Examples of the three layers of abstraction in XML configurations. (a) shows a definition of an electrode array. (b) shows the definition of an electrode. (c) shows the definition of an electrode group.

## User Interface

The user interface consists of a suite of three application that assist in the configuration, control, and monitoring of the electrode probe. All of the applications are written in Java 5.0 and rely on the XML files, library, and driver described above. The first application, called “Switch Monitor”, is used mainly for debugging. It continually polls the crosspoint switches for their states every 250 milliseconds. It displays whether a connection is made between each input and output in a grid. One can tile many switch monitors together, as in Figure 3-15(a), to see the state of many switches at once.

An application called “Electrode Designer” is designed to help define electrodes. This application can load the layout of an electrode array from a cell definition file, and display a representation of the array. The user can then click on the cells he wants in an electrode and save the configuration to an XML file of his choosing. A screenshot of a user in the process of defining electrodes for the square electrode probe

can be seen in Figure 3-15(b).

The “Electrode Controller” application is the application used to control the electrode probe while taking measurements. It uses information from all three layers of abstraction, as read from a file, to translate the user’s actions on the screen to commands that are sent to the electrode probe. The application shows a rendering of the electrode array to the user, and allows him to either choose a predefined electrode group to activate, or assign electrodes one by one, from drop down menus, to different outputs. A manual mode also allows the user to modify the connections cell by cell. A reset button is included as well to quickly turn off all of the connections and prevent any current to pass through the electrode array. A screen shot of this application can be seen in Figure 3-15(c).

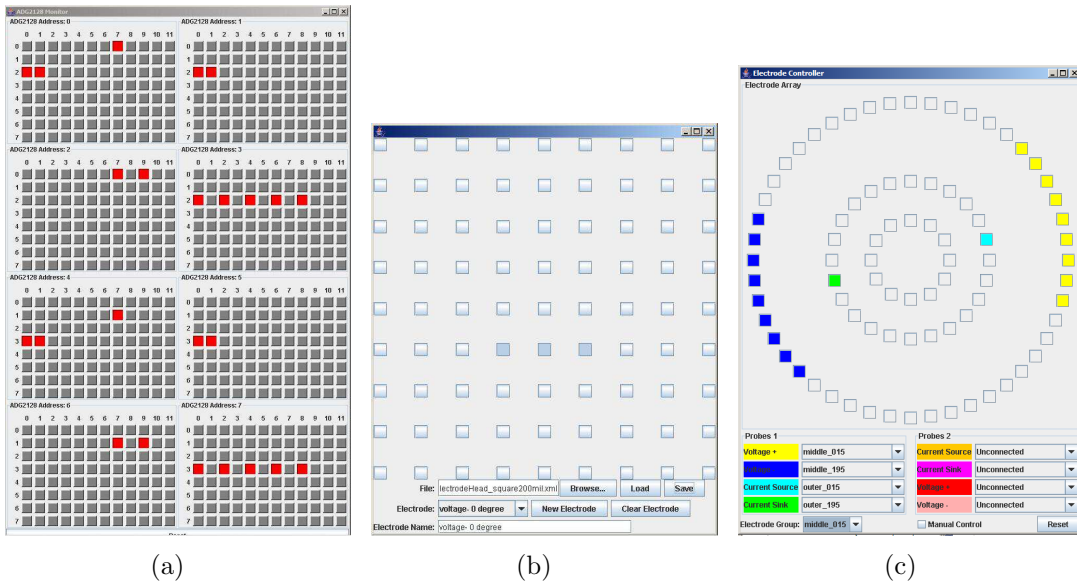


Figure 3-15: Screen shots of the electrode probe application suite: Switch Monitor (a), Electrode Designer (b), and Electrode Controller (c).

### 3.3.6 Performance

The electrode probe performed very well on balsa wood and was able to closely match the results obtained using electrode strips. Figure 3-16 shows the results for strips and the electrode probe with the small square array measuring the impedance of

balsa wood parallel to its grain. In these experiments the electrode strips were placed in the same positions as the corresponding cells in the electrode array. Results for perpendicular measurements were similar.

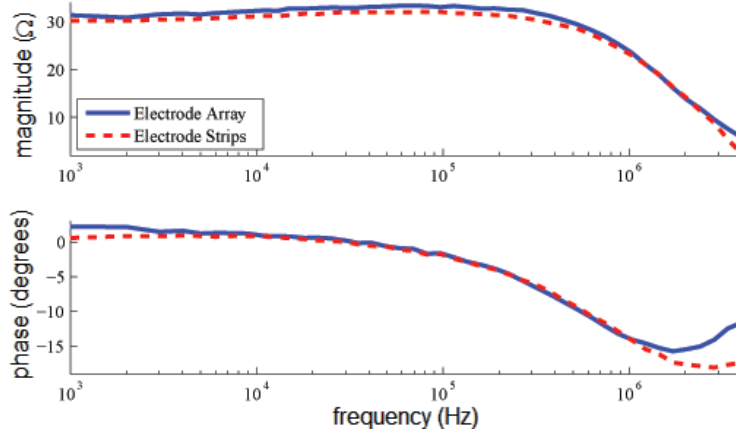


Figure 3-16: A comparison of balsa wood measurements made with the final electrode probe design and electrode strips. The measurements were made parallel to the wood grain, and a square electrode array was used.

The circular electrode array was also tested to demonstrate the ability of the electrode probe to perform a full rotational electrical impedance myography measurement. Measurements were taken at seven different angles, spaced in  $15^\circ$  intervals between the parallel and perpendicular orientations to the grain of the balsa wood. The results, in Figure 3-17, show that the impedance varied from a high when measuring perpendicular to the grain to a low when measuring parallel to the grain, as expected.

However, one may notice some unexpected results, especially when compared to the measurements taken with the square array, which must be explained. Perhaps the most striking difference is that the impedance of the parallel measurement in Figure 3-17 is much higher than in Figure 3-16. This occurred because the distance between the voltage electrodes used in the square array measurement was half the distance than in the circular array. The middle ring of electrodes was used in the circular array to allow for more angular measurements, and thus the diameter of the measurements had to be increased from 0.4" to 0.8".

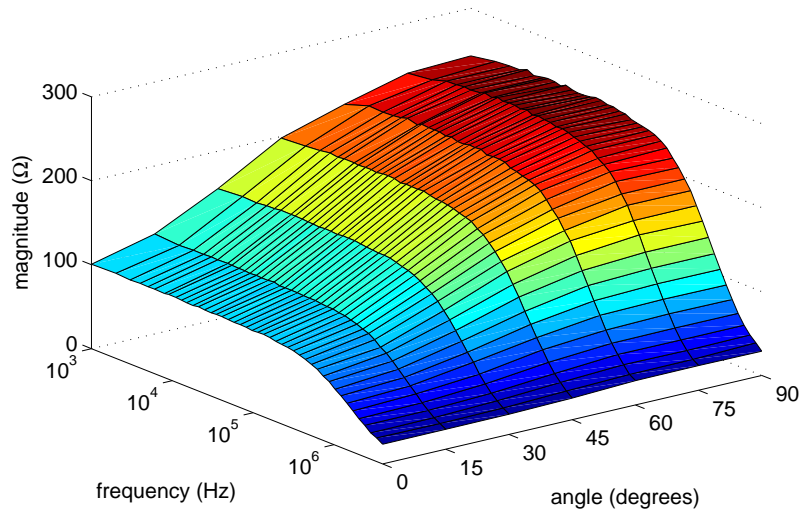


Figure 3-17: Rotational measurements of balsa wood with electrode probe.

The other unexpected result is that the impedance at 75° and 90° are almost identical. Although the 15° measurement is close to the 0° measurement as well, those two are much further apart. The reason for this phenomenon is unknown, but it could be due to the existence of an alternate, medium impedance, isotropic current path. Such a path would not have a significant effect when measuring impedance parallel to the grain of the wood since the parallel path would dominate. However, in the perpendicular case, the alternate current path's impedance could be comparable to the perpendicular path, and the measured impedance would be affected.



# Chapter 4

## Patient Safety

Patient safety is an extremely important concern of any medical device. Few things could be worse than having a device that is designed to help a patient actually harm him. Since there are many systems in the body that use electrical signaling to function properly, any device that applies an electric charge or current to the body has to take many precautions.

### 4.1 Cardiac Concerns

One of the main concerns with applying electrical energy to the body is that it may disturb the proper functioning of the heart. Although defibrillators (devices that intentionally disrupt malignant electrical activity in the heart) use hundreds of volts applied across the body there is still significant risk at much lower voltages. This is especially true about DC voltages that are applied over an extended period of time. The International Electrotechnical Commission specifies a maximum allowable current of  $100\mu A * f$ , where  $f$  is in kHz, for frequencies above 1 kHz [10].

The above guideline is meant to prevent ventricular fibrillation, so it is most applicable to currents traversing the chest and thus not an absolute limit for this application. However we should be mindful of this limit in our design, especially in trying to reduce low frequency current amplitude. DC current can be especially dangerous since it may cause voltage-controlled ion channels in neurons and muscle

cells to open, making the effected part of the body unable to function properly. To reduce the risk of this occurring we are driving the current electrodes completely differentially, removing the threat of a common-mode, DC, voltage. Not only does this make measurements easier to take accurately, but it also reduces the risk of injecting large amounts of low-frequency current into the body.

## 4.2 Isolation

Another precaution that is taken in the electrode design is electrically isolating the patient side of the device from high-voltage power lines. The probe has its own power supplied driven by two 9V batteries, with that supply reduced to +/-5V by voltage regulators. Since these rails power the crosspoint switches through which all electrode cells are connected, they limit the maximum voltage that can be applied to the patient to a largely harmless 10V spread.

## 4.3 Current Density

Tissue damage from burning is also a concern when current is applied to the body. The risk is not so much from the amount of current that is being applied, but rather from the current distribution. The body can handle a relatively large amount of current without permanent tissue damage if the current is spread out, but if it is concentrated on a small area the tissue may burn.

The maximum current density occurs at the points where it enters and exits the body, and it will spread out once in the body. As such, we want to increase the surface area of the current electrodes, but we must balance the need for larger electrodes with the desire for higher resolution of our electrode array. As discussed in Section 3.2.1 and [12], we gain extra safety from using an array of small electrodes as it produces a lower current distribution near the electrodes.

# Chapter 5

## Conclusion

This thesis presents a novel electrode probe and impedance measurement methods designed for electrical impedance myography. Electrical impedance myography has been shown to be a valuable diagnostic tool for neuromuscular diseases, but in its current state it is not ready to be widely accepted. The current technique is slow, uses large, expensive equipment, and requires a skilled technician to take measurements. Many of these problems are solved by work in this thesis.

The impedance measurement methods described have greatly increased the speed of multi-frequency analysis by examining all frequencies of interest simultaneously. A composite waveform, with 44 logarithmically spaced frequencies between 1 kHz and 4 MHz, is used to excite the muscle and make quick and accurate measurements. Differential circuits are used to inject current into the muscle, reducing the need for complicated common-mode rejection and improving patient safety.

A handheld electrode probe has also been made that enables quick and easy rotational measurements. The electrode probe uses an array of small electrodes that can be connected together in any configuration using analog crosspoint switches. The electrode array makes it possible to create virtual electrodes of any shape and orientation so that many angular measurements can be made without having to move the probe. The electrode probe has been designed to be as modular and expandable as possible so that electrode arrays of any configuration, size, and resolution can be swapped out for one another easily, depending on which is more appropriate for the

measurement at hand. The electrode probe can be controlled from a PC via a USB connection, and custom software has been written for this purpose. The software includes, firmware, drivers, and a suite of applications that make the probe easy to use and configure. The probe also contains an isolated power supply that ensures patient safety.

Together, the new measurement methods and electrode probe will propel electrical impedance myography to new levels of clinical acceptance and success. The improvements in speed, ease of use, and capability will allow for many interesting uses of electrical impedance myography that have not been explored yet such as the combination of dynamic and rotational methods.

Preliminary testing of the system has been done on materials with similar properties to muscle such as circuit models and balsa wood. The results have been very promising, showing good agreement to measurements taken using traditional methods.

## 5.1 Future Work

Although much work has been done in this thesis, there is still more that has yet to be done. Below are just a few of the projects that are in early stages of development at MIT's EIM Group.

- The measurement circuitry and systems will be integrated onto silicon, reducing many of the parasitic effects that are currently present in the system, as well as greatly reducing the overall bulk of the system.
- More research will be done on simultaneous multi-angular measurements. This will decrease the time needed to make a full angular characterization of muscle, to enable better temporal resolution for dynamic measurements.
- Clinical studies will begin using this system on animal and human subjects.

The future of electrical impedance myography looks very promising, especially with the development of the equipment and methods described here. It is my sincere

hope that this work will one day serve to reduce the suffering of the many people affected by neuromuscular disorders.



# Bibliography

- [1] R. Aaron, M. Huang, and C. Shiffman. Anisotropy of human muscle via non-invasive impedance measurements. *Physics in Medicine and Biology*, 42(7):1245–1262, 1997.
- [2] R. Aaron and C. A. Shiffman. Using localized impedance measurements to study muscle changes in injury and disease. *Annals of the New York Academy of Sciences*, 904:171–180, May 2000.
- [3] Agilent Technologies, 5301 Stevens Creek Blvd, Santa Clara, CA 95051, U.S.A. *Agilent Technologies Impedance Measurement Handbook*, December 2003.
- [4] Analog Devices, One Technology Way, P.O. Box 9106, Norwood, MA 02062-9106, U.S.A. *ADG2128 Datasheet: I2C CMOS 8 12 Unbuffered Analog Switch Array With Dual/Single Supplies*, May 2006.
- [5] A. Chin, S. Ruehr, A. Tarulli, and S. B. Rutkove. Saline-saturated balsa wood as a testing medium for rotational electrical impedance myography. In *Electrical Bioimpedance*. 13th International Conference on Electrical Bioimpedance, August 2007. To be published.
- [6] W. C. Chumlea and S. S. Guo. Bioelectrical impedance and body composition: Present status and future directions. *Nutrition Reviews*, 52(4):123–131, April 1994.
- [7] Cypress Semiconductor Corporation, 198 Champion Court, San Jose, CA 95134-1709, U.S.A. *CY7C68013A EZ-USB FX2LP USB Microcontroller High-Speed USB Peripheral Controller*, January 2006.
- [8] G. Esper, C. Shiffman, R. Aaron, K. Lee, and S. B. Rutkove. Assessing neuromuscular disease with multifrequency electrical impedance myography. *Muscle & Nerve*, 34(5):595–602, November 2006.
- [9] M. Hochman and J. Zilberfarb. Nerves in a pinch: imaging of nerve compression syndromes. *Radiologic Clinics of North America*, 42(1):221–245, January 2004.
- [10] IEC 60601-1. *Medical Electrical Equipment: I-II. General Requirements for Basic Safety and Essential Performance—Collateral Standard: Electromagnetic Compatibility—Requirements and Tests*, 3 edition, 2007.

- [11] A. LeBlanc, R. Rowe, H. Evans, S. West, L. Shackelford, and Victor Schneider. Muscle atrophy during long duration bed rest. *International Journal of Sports Medicine*, 18:S283–S285, 1997.
- [12] L. Livshitz, J. Mizrahi, and P. Einziger. Interaction of array of finite electrodes with layered biological tissue: Effect of electrode size and configuration. *IEEE Transactions On Neural Systems And Rehabilitation Engineering*, 9(4):355–361, December 2001.
- [13] K. D. Mathews. Muscular dystrophy overview: Genetics and diagnosis. *Neurologic Clinics*, 21(4):795–816, November 2003.
- [14] A. McEwan, G. Cusick, and D. S. Holder. A review of errors in multi-frequency eit instrumentation. *Physiological Measurement*, 28:S197–S215, June 2007.
- [15] R. Nie, N. A. Sunmonu, A. B. Chin, K. S. Lee, and S. B. Rutkove. Electrical impedance myography: Transitioning from human to animal studies. *Clinical Neurophysiology*, 117(8):1844–1849, June 2006.
- [16] A. Pitt, J. Fleckenstein, R. Greenlee Jr., D. Burns, W. Bryan, and R. Haller. Mri-guided biopsy in inflammatory myopathy: initial results. *Magnetic Resonance Imaging*, 11:1093–1099, 1993.
- [17] C. Reimers, J. Fleckenstein, T. Witt, W. Muller-Felber, and D. Pongratz. Muscular ultrasound in idiopathic inflammatory myopathies of adults. *Journal of Neurology*, 116(1):82–92, May 1993.
- [18] S. B. Rutkove, R. Aaron, and C. Shiffman. Localized bioimpedance analysis in the evaluation of neuromuscular disease. *Muscle & Nerve*, 25(3):390–397, March 2002.
- [19] C. A. Shiffman and R. Aaron. Angular dependence of resistance in non-invasive electrical measurements of human muscle: The tensor model. *Physics in Medicine and Biology*, 43(5):1317–1323, 1998.
- [20] C. A. Shiffman, R. Aaron, and S. B. Rutkove. Electrical impedance of muscle during isometric contraction. *Physiological Measurement*, 24:213–234, February 2003.
- [21] Tektronix, 14200 SW Karl Braun Drive, P.O. Box 500, Beaverton, OR 97077, U.S.A. *Digital Phosphor Oscilloscopes: TDS300B Series*, February 2006.
- [22] Tektronix, 14200 SW Karl Braun Drive, P.O. Box 500, Beaverton, OR 97077, U.S.A. *Arbitrary Function Generators*, June 2007.